Metal−Metal Bonding in Pentanuclear Bow-Tie Metal Sulfido Clusters. Synthetic and Structural Studies on the Cationic Pentanuclear Clusters $[(Cp^*Ir)_2(\mu_3\text{-}S)_2M(\mu_3\text{-}S)_2(IrCp^*)_2]^{n+}$ (M = Fe, Co, Ni; n = 1, 2)

Zhen Tang,[†] Yasuo Nomura,[†] Shigeki Kuwata,[†] Youichi Ishii,[†] Yasushi Mizobe,[‡] and Masanobu Hidai*,[†]

Department of Chemistry and Biotechnology, Graduate School of Engineering, The University of Tokyo, Hongo, Bunkyo-ku, Tokyo 113-8656, Japan, and Institute of Industrial Science, The University of Tokyo, Roppongi, Minato-ku, Tokyo 106-8558, Japan

Received June 18, 1998

Reactions of $[Cp^*MCl(\mu_2\text{-}SH)_2MCp^*Cl]$ (**1**, M = Ir; **2**, M = Rh; $Cp^* = \eta^5\text{-}C_5Me_5$) with excess $FeCl_2\cdot 4H_2O$ in THF gave the paramagnetic trinuclear clusters $[(Cp^*M)_2(\mu_3\text{-}S)_2FeCl_2]$ (**3**, M = Ir; **4**, M = Rh), which were further converted into the dicationic 78e$^-$ pentanuclear bow-tie cluster $[(Cp^*Ir)_2(\mu_3\text{-}S)_2Fe(\mu_3\text{-}S)_2(IrCp^*)_2]^{2+}$ (**5**) by treatment with $NaBPh_4$. When complex **1** was allowed to react with $CoCl_2$ and $NiCl_2\cdot 6H_2O$ or Ni(cod)$_2$ (cod = cyclooctadiene), the related pentanuclear 79e$^-$ and 80e$^-$ bow-tie clusters $[(Cp^*Ir)_2(\mu_3\text{-}S)_2M(\mu_3\text{-}S)_2(IrCp^*)_2]^{2+}$ (**6**, M = Co; **7**, M = Ni) were obtained directly, respectively. Cyclic voltammograms of **5**$[BPh_4]_2$, **6**$[BPh_4]_2$, and **7**$[BPh_4]_2$ showed two reversible reduction waves at −0.25 to −0.43 V and −1.04 to −1.34 V. In both redox couples, the redox potential was in the order Fe < Co < Ni. One-electron reduction of clusters **5**$[BPh_4]_2$, **6**$[BPh_4]_2$, and **7**$[BPh_4]_2$ with Co($\eta^5\text{-}C_5H_5)_2$ gave the corresponding monocationic pentanuclear 79−81e$^-$ bow-tie clusters $[(Cp^*Ir)_2(\mu_3\text{-}S)_2M(\mu_3\text{-}S)_2(IrCp^*)_2]^+$ (**8**, M = Fe; **9**, M = Co; **10**, M = Ni). The molecular structures of **3**, **4**, **5**$[BPh_4]_2\cdot CH_2Cl_2$, **6**$[CoCl_3(NCMe)]_2$, **7**$[NiCl_4]\cdot CH_2Cl_2$, **8**$[BPh_4]$, **9**$[BPh_4]$, and **10**$[BPh_4]$ were unambiguously determined by X-ray diffraction study. The structures of the pentanuclear bow-tie cluster cores remarkably changed stepwise as the core electrons increased from 78 to 81. Two of the M−Ir (M = Fe, Co) bonds in the 79e$^-$ clusters **6** and **8** show significant elongation in comparison with the Fe−Ir bonds in the 78e$^-$ cluster **5**. Two different types of the bow-tie structures were observed for the 80e$^-$ clusters **7** and **9**. Cluster **7** has a Z-shaped metal core with only two Ni−Ir bonds, while in cluster **9**, the six metal−metal bonds in the bow-tie structure are retained with slight elongation of the Co−Ir bonds in comparison with the corresponding dication **6**. The 81e$^-$ cluster **10** has two normal Ni−Ir bonds and one long Ni−Ir bonding interaction with the fourth nonbonding Ni−Ir contact. This structural variation is interpreted in terms of the total electron counts and molecular orbital calculations of the clusters.

Introduction

Transition-metal clusters with sulfur-based ligands have received wide attention[1] because of their relevance to biochemical processes promoted by metalloproteins[2] and industrial processes by heterogeneous metal sulfide catalysts.[3] Considerable efforts have been devoted to the synthetic and structural studies on sulfido and thiolato clusters of metals related to the biological and industrial systems, for example, those of iron and molybdenum. However, the chemistry of noble metal sulfur clusters has been much less extensively investigated despite their potential as a new class of catalysts in organic synthesis.[4]

We have continuously been interested in the preparation and reactivities of groups 8−10 noble metal sulfur clusters over the past fifteen years, and have developed multinuclear sulfido and thiolato complexes of ruthenium,[5] iridium,[6] and palladium,[7]

[†] Department of Chemistry and Biotechnology.
[‡] Institute of Industrial Science.

(1) For recent reviews: (a) Mathur, P. *Adv. Organomet. Chem.* **1997**, *41*, 243. (b) Dance, I.; Fisher, K. *Prog. Inorg. Chem.* **1994**, *41*, 637. (c) Saito, T. In *Early Transition Metal Clusters with π-Donor Ligands*; Chisholm, M. H., Ed.; VCH: New York, 1995; Chapter 3. (d) Shibahara, T. *Coord. Chem. Rev.* **1993**, *123*, 73. (e) Krebs, B.; Henkel, G. *Angew. Chem., Int. Ed. Engl.* **1991**, *30*, 769. (f) Holm, R. H.; Ciurli, S.; Weigel, J. A. *Prog. Inorg. Chem.* **1990**, *38*, 1.

(2) (a) Rees, D. C.; Chan, M. K.; Kim, J. *Adv. Inorg. Chem.* **1994**, *40*, 89. (b) Coucouvanis, D. In *Molybdenum Enzymes, Cofactors, and Model Systems*; Stiefel, E. I., Coucouvanis, D., Newton, W. E., Eds.; American Chemical Society: Washington, DC, 1993; p 304. (c) *Adv. Inorg. Chem.* **1992**, *38*.

(3) (a) Angelici, R. J. *Acc. Chem. Res.* **1988**, *21*, 387. (b) Chen, J.; Daniels, L. M.; Angelici, R. J. *J. Am. Chem. Soc.* **1990**, *112*, 199. (c) Wiegand, B. C.; Friend, C. M. *Chem. Rev.* **1992**, *92*, 491. (d) Riaz, V.; Curnow, O. J.; Curtis, M. D. *J. Am. Chem. Soc.* **1994**, *116*, 4357. (e) Bianchini, C.; Meli, A. *J. Chem. Soc., Dalton Trans.* **1996**, 801.

(4) Rakowski DuBois, M. *Chem. Rev.* **1989**, *89*, 1.

(5) (a) Hidai, M.; Imagawa, K.; Cheng, G.; Mizobe, Y.; Wakatsuki, Y.; Yamazaki, H. *Chem. Lett.* **1986**, 1299. (b) Dev, S.; Imagawa, K.; Mizobe, Y.; Cheng, G.; Wakatsuki, Y.; Yamazaki, H.; Hidai, M. *Organometallics* **1989**, *8*, 1232. (c) Dev, S.; Mizobe, Y.; Hidai, M. *Inorg. Chem.* **1990**, *29*, 4797. (d) Takahashi, A.; Mizobe, Y.; Matsuzaka, H.; Dev, S.; Hidai, M. *J. Organomet. Chem.* **1993**, *456*, 243.

(6) (a) Nishio, M.; Matsuzaka, H.; Mizobe, Y.; Hidai, M. *Angew. Chem., Int. Ed. Engl.* **1996**, *35*, 872. (b) Nishio, M.; Matsuzaka, H.; Mizobe, Y.; Hidai, M. *Inorg. Chim. Acta* **1997**, *263*, 119. (c) Nishio, M.; Mizobe, Y.; Matsuzaka, H.; Hidai, M. *Inorg. Chim. Acta* **1997**, *265*, 59.

(7) (a) Murata, T.; Gao, H.; Mizobe, Y.; Nakano, F.; Motomura, S.; Tanase, T.; Yano, S.; Hidai, M. *J. Am. Chem. Soc.* **1992**, *114*, 8287. (b) Murata, T.; Mizobe, Y.; Gao, H.; Ishii, Y.; Wakabayashi, T.; Nakano, F.; Tanase, T.; Yano, S.; Hidai, M.; Echizen, I.; Nanikawa H.; Motomura, S. *J. Am. Chem. Soc.* **1994**, *116*, 3389.

S0020-1669(98)00688-0 CCC: $15.00
Published on Web 08/26/1998

which showed intriguing stoichiometric reactivities[8] and catalytic activities[7b,9] toward various types of substrates such as alkynes, alkyl halides, allylic alcohols, aldehydes, and hydrazines. In this series of works, we have recently synthesized the dinuclear hydrosulfido complexes $[Cp^*MCl(\mu_2\text{-}SH)_2MCp^*Cl]$ (M = Ru, Ir, Rh; $Cp^* = \eta^5\text{-}C_5Me_5$), which provide versatile precursors for various tri- and tetranuclear sulfido clusters.[10,11] In particular, reactions of $[Cp^*MCl(\mu_2\text{-}SH)_2MCp^*Cl]$ (M = Ru, Ir) with other transition-metal complexes led to the formation of heterobimetallic trinuclear clusters in high yields, which include $[(Cp^*Ru)_2(\mu_2\text{-}H)(\mu_3\text{-}S)_2RhCl_2(PPh_3)]$,[10] $[(Cp^*Ir)_2(\mu_3\text{-}S)_2Rh(cod)]^+$ (cod = cyclooctadiene),[11a] and $[(Cp^*Ir)_2(\mu_3\text{-}S)_2PdCl(PPh_3)]^+$.[11a] It is noteworthy that the $Cp^*M(\mu_3\text{-}S)_2MCp^*$ (M = Ru, Ir) fragment derived from the hydrosulfido complexes may be regarded as a potential metalloligand. We envisaged that these hydrosulfido complexes can be used for further construction of a wide variety of platinum metal sulfido cluster cores, especially those of higher nuclearity. Now we have found that the mono- and dicationic pentanuclear bow-tie clusters $[(Cp^*Ir)_2(\mu_3\text{-}S)_2M(\mu_3\text{-}S)_2(IrCp^*)_2]^{n+}$ (M = Fe, Co, Ni; $n = 1$, 2) are readily synthesized from $[Cp^*IrCl(\mu_2\text{-}SH)_2IrCp^*Cl]$ (**1**). Those clusters, which provide rare examples of $78-81e^-$ bow-tie clusters, show interesting structural changes depending upon their electron counts.

It is widely accepted that the number of metal−metal bonds in cluster complexes corresponds with their total electron counts.[12] Metal sulfur clusters are expected to provide excellent systems for the study on structural changes of polynuclear complexes triggered by perturbation in their electronic states, because sulfur-based ligands behave as effective bridging ligands and prevent the cluster cores from fragmenting into metal species of lower nuclearity on redox reactions. In this context, the cluster core structures of trigonal bipyramidal trinuclear clusters such as $[(p\text{-cymene})_3M_3S_2]^{n+}$ (M = Ru, Os; $n = 0$, 2),[13] $[Co_3(C_5H_4Me)_3S_2]^{n+}$ ($n = 0,1,2$),[14] and $[Cp^*{}_3Ir_3S_2]^{n+}$ ($n = 0$, 2)[15] and cuboidal tetranuclear clusters such as $[(C_5H_4R)_4Ru_4E_4]^{n+}$ (E = S, Se, Te; R = Me, $SiMe_3$; $n = 0$, 2),[16] $[Cp^*{}_4Ir_4S_4]^{n+}$ ($n = 0$, 2),[15] and $[(C_5H_4Me)_2Mo_2M_2S_4(CO)_2]^{n-}$ (M = Co, Ni; $n = 0$, 1) and their derivatives[17] have been extensively investigated so far and shown to correlate nicely with their total electron counts. In contrast, relationship between electronic states and metal−metal bond cleavage and formation in sulfido clusters with much higher nuclearity has been investigated less systematically.

Among pentanuclear clusters, the bow-tie clusters, in which the five metal atoms are arranged in the form of two triangular M_3 units sharing the central metal atom, form a unique class of clusters. A considerable number of compounds of this type have been synthesized and crystallographically determined so far,[18−20] most of which are limited to $72-78e^-$ species.[18,19] If the cluster has 78 valence electrons, the cluster core is expected to have most typically six metal−metal single bonds. However, no systematic study has been reported about the structural change caused by stepwise increase of the valence electrons from a $78e^-$ bow-tie cluster.[19] In this paper, we describe the syntheses and structures of a series of pentanuclear bow-tie clusters $[(Cp^*Ir)_2(\mu_3\text{-}S)_2M(\mu_3\text{-}S)_2(IrCp^*)_2]^{n+}$ (M = Fe, Co, Ni; $n = 1$, 2), which illustrate the correlation between the cluster electron counts and the core structures of $78-81e^-$ clusters.

Results and Discussion

Syntheses and Structures of $[(Cp^*M)_2(\mu_3\text{-}S)_2FeCl_2]$ (M = Ir, Rh). In the previous paper, we reported that the hydrosulfido-bridged diiridium and dirhodium complexes $[Cp^*MCl(\mu_2\text{-}SH)_2MCp^*Cl]$ (**1**, M = Ir; **2**, M = Rh) react with several noble

(8) (a) Hidai, M.; Mizobe, Y.; Matsuzaka, H. *J. Organomet. Chem.* **1994**, *473*, 1 and references therein. (b) Matsuzaka, H.; Takagi, Y.; Hidai, M. *Organometallics* **1994**, *13*, 13. (c) Nishio, M.; Matsuzaka, H.; Mizobe, Y.; Tanase, T.; Hidai, M. *Organometallics* **1994**, *13*, 4214. (d) Takahashi, A.; Mizobe, Y.; Tanase, T.; Hidai, M. *J. Organomet. Chem.* **1995**, *496*, 109. (e) Nishio, M.; Matsuzaka, H.; Mizobe, Y.; Hidai, M. *Organometallics* **1996**, *15*, 965. (f) Mizobe, Y.; Hosomizu, M.; Kubota, Y.; Hidai, M. *J. Organomet. Chem.* **1996**, *507*, 179. (g) Takagi, Y.; Matsuzaka, H.; Ishii, Y.; Hidai, M. *Organometallics* **1997**, *16*, 4445.

(9) (a) Hidai, M.; Mizobe, Y. In *Transition Metal Sulfur Chemistry: Biological and Industrial Significance;* Stiefel, E. I., Matsumoto, K., Eds.; ACS Symposium Series 653; American Chemical Society: Washington, DC, 1996; p 310. (b) Kuwata, S.; Mizobe, Y.; Hidai, M. *Inorg. Chem.* **1994**, *33*, 3619. (c) Shimada, H.; Qü, J.; Matsuzaka, H.; Ishii, Y.; Hidai, M. *Chem. Lett.* **1995**, 671. (d) Matsuzaka, H.; Takagi, Y.; Ishii, Y.; Nishio, M.; Hidai, M. *Organometallics* **1995**, *14*, 2153. (e) Wakabayashi, T.; Ishii, Y.; Murata, T.; Mizobe Y.; Hidai, M. *Tetrahedron Lett.* **1995**, *36*, 5585. (f) Wakabayashi, T.; Ishii, Y.; Ishikawa, K.; Hidai, M. *Angew. Chem., Int. Ed. Engl.* **1996**, *35*, 2123. (g) Nishibayashi, Y.; Yamanashi, M.; Takagi, Y.; Hidai, M. *Chem. Commun.* **1997**, 859.

(10) Hashizume, K.; Mizobe, Y.; Hidai, M. *Organometallics* **1996**, *15*, 3303.

(11) (a) Tang, Z.; Nomura, Y.; Ishii, Y.; Mizobe Y.; Hidai, M. *Organometallics* **1997**, *16*, 151. (b)Tang, Z.; Nomura, Y.; Ishii, Y.; Mizobe Y.; Hidai, M. *Inorg. Chim. Acta* **1998**, *267*, 73.

(12) Mingos, D. M. P.; May, A. S. In *The Chemistry of Metal Cluster Complexes*; Shriver, D. F., Kaesz, H. D., Adams, R. D., Eds.; VCH: New York, 1990; Chapter 2.

(13) Lockemeyer, J. R.; Rauchfuss, T. B.; Rheingold, A. L. *J. Am. Chem. Soc.* **1989**, *111*, 5733.

(14) Pulliam, C. R.; Thoden, J. B.; Stacy, A. M.; Spencer, B.; Englert, M. H.; Dahl, L. F. *J. Am. Chem. Soc.* **1991**, *113*, 7398.

(15) Venturelli, A.; Rauchfuss, T. B. *J. Am. Chem. Soc.* **1994**, *116*, 4824.

(16) Houser, E. J.; Rauchfuss, T. B.; Wilson, S. R. *Inorg. Chem.* **1993**, *32*, 4069.

(17) (a) Curtis, M. D.; Williams, P. D.; Butler, W. M. *Inorg. Chem.* **1988**, *27*, 2853. (b) Curtis, M. D.; Druker, S. H.; Goossen, L.; Kampf, J. W. *Organometallics* **1997**, *16*, 231. (c) Mansour, M. A.; Curtis, M. D.; Kampf, J. W. *Organometallics* **1997**, *16*, 3363.

(18) (a) Adams, R. D.; Horváth, I. T.; Yang, L.-W. *Organometallics* **1983**, *2*, 1257. (b) Bolinger, C. M.; Weatherill, T. D.; Rauchfuss, T. B.; Rheingold, A. L.; Day, C. S.; Wilson, S. R. *Inorg. Chem.* **1986**, *25*, 634. (c) Eremenko, I. L.; Pasynskii, A. A.; Katugin, A. S.; Zalmanovitch, V. R.; Orazsakhatov, B.; Sleptsova, S. A.; Nekhaev, A. I.; Kaverin, V. V.; Ellert, O. G.; Novotortsev, V. M.; Yanovsky, A. I.; Shklover, V. E.; Struchkov, Yu. T. *J. Organomet. Chem.* **1989**, *365*, 325. (d) Holliday, R. L.; Roof, L. C.; Hargus, B.; Smith, D. M.; Wood, P. T.; Pennington, W. T.; Kolis, J. W. *Inorg. Chem.* **1995**, *34*, 4392. (e) Calderoni, F.; Demartin F.; Iapalucci, M. C.; Laschi, F.; Longoni, G.; Zanello, P. *Inorg. Chem.* **1996**, *35*, 898. Also see ref 12.

(19) Pasynskii et al. have reported a series of bow-tie clusters with 72−75 valence electrons, $[\{(C_5H_4R)_2Cr_2(\mu_2\text{-}SBu^t)(\mu_3\text{-}S)_2\}_2M]$ (M = Cr, Mn, Fe, Co; R = H, Me) and $[\{Cp_2Cr_2(\mu_2\text{-}SBu^t)(\mu_3\text{-}S)_2\}_2Fe]^+$, but the correlation of the cluster core structures of these complexes with their valence electron counts is obscure. (a) Pasynskii, A. A.; Eremenko, I. L.; Orazsakhatov, B.; Gasanov, G. Sh.; Shklover, V. E.; Struchkov, Yu. T. *J. Organomet. Chem.* **1984**, *269*, 147. (b) Eremenko, I. L.; Pasynskii, A. A.; Gasanov, G. Sh.; Orazsakhatov, B.; Struchkov, Yu. T.; Shklover, V. E. *J. Organomet. Chem.* **1984**, *275*, 71. (c) Eremenko, I. L.; Pasynskii, A. A.; Gasanov, G. Sh.; Orazsakhatov, B.; Struchkov, Yu. T.; Shklover, V. E. *J. Organomet. Chem.* **1984**, *275*, 183. (d) Pasynskii, A. A.; Eremenko, I. L.; Gasanov, G. Sh.; Struchkov, Yu. T.; Shklover, V. E. *J. Organomet. Chem.* **1984**, *276*, 349. (e) Pasynskii, A. A.; Eremenko, I. L.; Stomakhina, E. E.; Nefedov, S. E.; Ellert, O. G.; Yanovsky, A. I.; Struchkov, Yu. T. *J. Organomet. Chem.* **1991**, *406*, 383.

(20) (a) Eldredge, P. A.; Bose, K. S.; Barber, D. E.; Bryan, R. F.; Sinn, E.; Rheingold, A.; Averill, B. A. *Inorg. Chem.* **1991**, *30*, 2365. (b) Van den Berg, W.; Boot, C. E.; Van der Linden, J. G. M.; Bosman, W. P.; Smits, J. M. M.; Beurskens, P. T.; Heck, J. *Inorg. Chim. Acta* **1994**, *216*, 1. (c) Barber, D. E.; Sabat, M.; Sinn, E.; Averill, B. A. *Organometallics*, **1995**, *14*, 3229. (d) Mathur, P.; Sekar, P. *Chem. Commun.* **1996**, 727. (e) Van den Berg, W.; Boot, L.; Joosen H.; Van der Linden, J. G. M.; Bosman, W. P.; Smits, J. M. M.; De Gelder, R.; Beurskens, P. T.; Heck, J.; Gal, A. W. *Inorg. Chem.* **1997**, *36*, 1821. (f) Mathur, P.; Sekar, P.; Rheingold, A. L.; Liable-Sands, L. M. *J. Chem. Soc., Dalton Trans.* **1997**, 2949.

Table 1. Selected Interatomic Distances and Angles in **3** and **4**

3		**4**	
	Bond Distances (Å)		
Ir(1)−Ir(2)	2.807(1)	Rh(1)−Rh(2)	2.7835(8)
Ir(1)−Fe(1)	2.880(3)	Rh(1)−Fe(1)	2.837(1)
Ir(2)−Fe(1)	3.006(3)	Rh(2)−Fe(1)	2.954(1)
Ir(1)−S(1)	2.328(6)	Rh(1)−S(1)	2.315(2)
Ir(1)−S(2)	2.280(5)	Rh(1)−S(2)	2.307(2)
Ir(2)−S(1)	2.289(5)	Rh(2)−S(1)	2.303(2)
Ir(2)−S(2)	2.290(5)	Rh(2)−S(2)	2.294(2)
Fe(1)−Cl(1)	2.257(7)	Fe(1)−Cl(1)	2.253(2)
Fe(1)−Cl(2)	2.241(8)	Fe(1)−Cl(2)	2.229(2)
Fe(1)−S(1)	2.336(6)	Fe(1)−S(1)	2.310(2)
Fe(1)−S(2)	2.339(6)	Fe(1)−S(2)	2.296(2)
	Bond Angles (deg)		
Ir(2)−Ir(1)−Fe(1)	63.81(7)	Rh(2)−Rh(1)−Fe(1)	63.40(3)
Ir(1)−Ir(2)−Fe(1)	59.28(7)	Rh(1)−Rh(2)−Fe(1)	59.18(2)
Ir(1)−Fe(1)−Ir(2)	56.91(6)	Rh(1)−Fe(1)−Rh(2)	57.41(2)
S(1)−Ir(1)−S(2)	87.4(2)	S(1)−Rh(1)−S(2)	88.06(6)
S(1)−Ir(2)−S(2)	88.1(2)	S(1)−Rh(2)−S(2)	88.66(7)
S(1)−Fe(1)−S(2)	85.8(2)	S(1)−Fe(1)−S(2)	88.43(7)

metal complexes to give trinuclear sulfido clusters with the metalloligand $Cp^*M(\mu_2\text{-}S)_2MCp^*$.[11a] Aiming at establishing a rational synthetic method for heterobimetallic metal clusters starting from complexes **1** and **2**, we have now investigated their reactions with first-row transition metal compounds. Treatment of **1** with $FeCl_2 \cdot 4H_2O$ in THF at room temperature afforded the trinuclear cluster $[(Cp^*Ir)_2(\mu_3\text{-}S)_2FeCl_2]$ (**3**) in high yield. Concomitant formation of two molecules of HCl per one molecule of **1** was confirmed by isolation of $HNEt_3Cl$ from the reaction mixture by neutralization of the volatile acidic products with NEt_3. The rhodium analogue **2** reacted similarly with $FeCl_2 \cdot 4H_2O$, but the yield of $[(Cp^*Rh)_2(\mu_3\text{-}S)_2FeCl_2]$ (**4**) was moderate (eq 1).

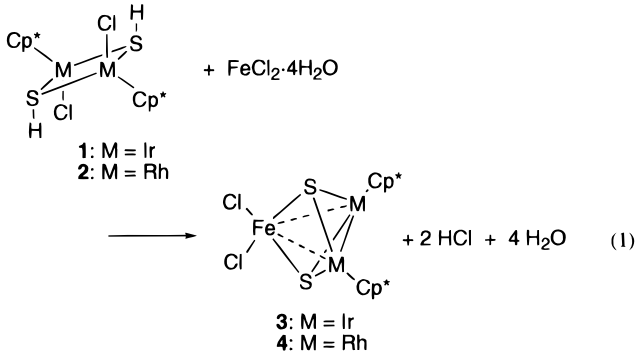

(1)

The molecular structures of **3** and **4** were unambiguously determined by X-ray crystallography. The ORTEP views of **3** and **4** are given in Figure 1, and their selected bond distances and angles are summarized in Table 1. Cluster **3** has a triangular $46e^-$ Ir_2Fe core, which is capped by the μ_3-sulfido ligands from both sides. The Ir−Ir distance of 2.807(1) Å falls in the range of Ir−Ir single bond distances,[21] while the Ir−Fe contacts of 2.880(3) and 3.006(3) Å, especially the latter, are significantly

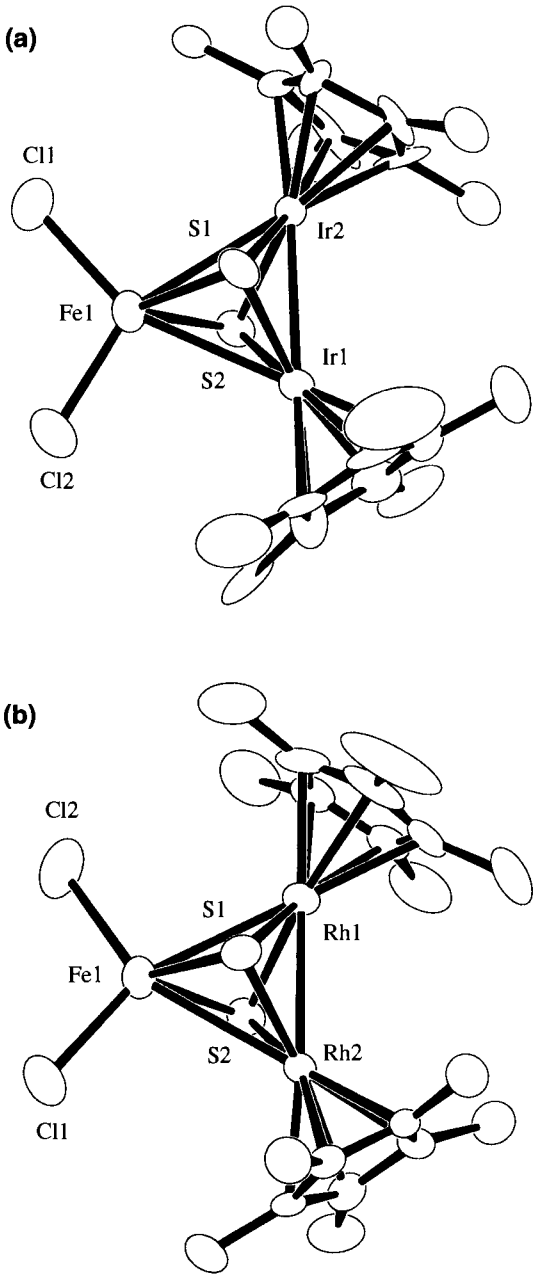

Figure 1. Molecular structures of **3** (a) and **4** (b). Hydrogen atoms are omitted for clarity.

longer than common Ir−Fe single bond distances (2.55−2.80 Å),[21c−e,22] indicating that the interatomic interaction between the iron and iridium atoms is weak. If the Ir−Fe contacts are neglected, the geometry around the iron atom is tetrahedral. Cluster **4** exhibits a closely related structure to that of **3**, where the respective metal−metal distances in **4** (Rh−Rh, 2.7835(8) Å; Rh−Fe, 2.837(1) and 2.954(1) Å) are slightly shorter than those in **3**.

Clusters **3** and **4** are paramagnetic at room temperature. The magnetic susceptibility measurement for **3** in the solid state at 18 °C gave a value for the effective magnetic moment μ_{eff} of 5.22 μ_B, which corresponds to the high spin state ($S = 2$) of the Fe(II) center. In the ^1H NMR spectra of **3** and **4** in $CDCl_3$

(21) (a) Mueting, A. M.; Boyle, P. D.; Wagner, R.; Pignolet, L. H. *Inorg. Chem.* **1988**, *27*, 271. (b) Bright, T. A.; Jones, R. A.; Koschmieder, S. U.; Nunn, C. M. *Inorg. Chem.* **1988**, *27*, 3819. (c) Pergola, R. D.; Garlaschelli, L.; Demartin, F.; Manassero, M.; Masciocchi, N.; Sansoni, M. *J. Chem. Soc., Dalton Trans.* **1990**, 127. (d) Bruce, M. I.; Koutsantonis, G. A.; Tiekink, E. R. T. *J. Organomet. Chem.* **1991**, *407*, 391. (e) Pergola, R. D.; Ceriotti, A.; Garlaschelli, L.; Demartin, F.; Manassero, M.; Masciocchi, N.; Sansoni, M. *Inorg. Chem.* **1993**, *32*, 3277. (f) Jones, W. D.; Chin, R. M. *J. Am. Chem. Soc.* **1994**, *116*, 198. (g) Vicic, D. A.; Jones, W. D. *Organometallics* **1997**, *16*, 1912.

(22) (a) Rosenberg, S.; Mahoney, W. S.; Hayes, J. M.; Geoffroy, G. L.; Rheingold, A. L. *Organometallics* **1986**, *5*, 1065. (b) Crespi, A. M.; Sabat, M.; Shriver, D. F. *Inorg. Chem.* **1988**, *27*, 812. (c) Chen, J.; Daniels, L. M.; Angelici, R. J. *J. Am. Chem. Soc.* **1991**, *113*, 2544.

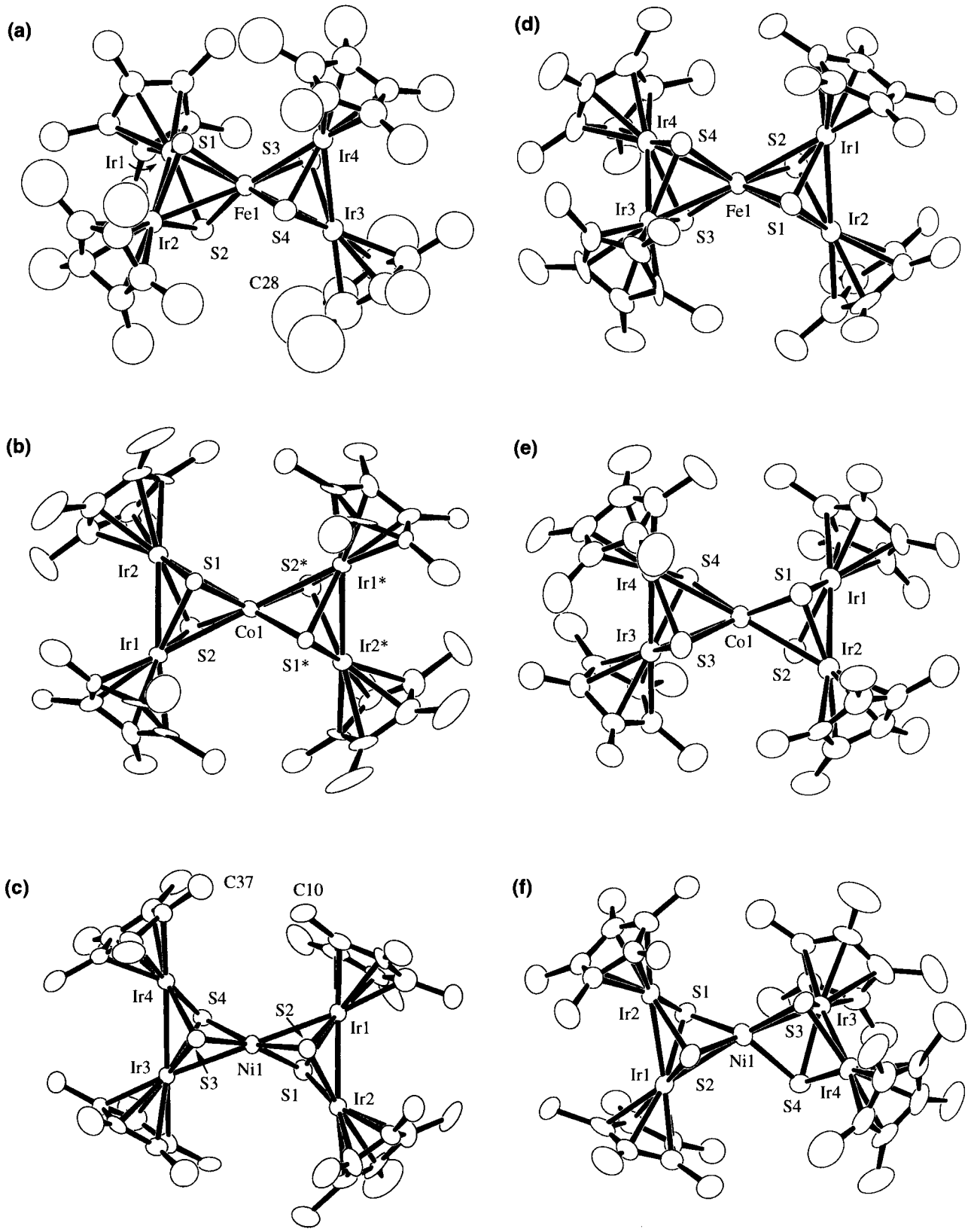

Figure 2. Structures of the cationic parts in **5**$[BPh_4]_2 \cdot CH_2Cl_2$ (a), **6**$[CoCl_3(NCMe)]_2$ (b), **7**$[NiCl_4] \cdot CH_2Cl_2$ (c), **8**$[BPh_4]$ (d), **9**$[BPh_4]$ (e), and **10**$[BPh_4]$ (f). Hydrogen atoms are omitted for clarity.

at room temperature, the Cp* signals appeared at δ −30.86 and −30.94, respectively. The Cp* proton signal for cluster **3** displays further upfield shift as the temperature was lowered. Preliminary investigation of the temperature dependence of the ^{1}H NMR spectrum of **3** revealed an excellent linear correlation between the isotropic shift and inverse temperature ($1/T$) over the temperature range of −50−25 °C. Extrapolation to infinite temperature ($1/T = 0$) led to a reasonable value (δ 1.51) of the diamagnetic shift for the Cp* signal.[23] These observations are consistent with the Curie law. Similar strong upfield shifts have been reported for the 46e$^-$ triangular clusters $[(Cp^*M)_n(\mu\text{-}CO)_2(CoCp)_{3-n}]$ (M = Co, Rh, Ir; n = 1, 2; Cp = η^5-C_5H_5).[24]

Table 2. Selected Interatomic Distances and Angles in $\mathbf{5}[BPh_4]_2\cdot CH_2Cl_2$

Bond Distances (Å)			
Ir(1)−Ir(2)	2.7877(8)	Ir(3)−Ir(4)	2.7736(8)
Ir(1)−Fe(1)	2.700(2)	Ir(2)−Fe(1)	2.727(2)
Ir(3)−Fe(1)	2.707(2)	Ir(4)−Fe(1)	2.725(2)
Ir(1)−S(1)	2.279(3)	Ir(1)−S(2)	2.279(3)
Ir(2)−S(1)	2.279(3)	Ir(2)−S(2)	2.278(3)
Ir(3)−S(3)	2.280(4)	Ir(3)−S(4)	2.274(3)
Ir(4)−S(3)	2.266(3)	Ir(4)−S(4)	2.278(3)
Fe(1)−S(1)	2.164(3)	Fe(1)−S(2)	2.171(4)
Fe(1)−S(3)	2.162(4)	Fe(1)−S(4)	2.161(4)
Bond Angles (deg)			
Ir(2)−Ir(1)−Fe(1)	59.56(4)	Ir(1)−Ir(2)−Fe(1)	58.62(4)
Ir(4)−Ir(3)−Fe(1)	59.63(4)	Ir(3)−Ir(4)−Fe(1)	58.97(4)
Ir(1)−Fe(1)−Ir(2)	61.81(4)	Ir(1)−Fe(1)−Ir(3)	144.08(7)
Ir(1)−Fe(1)−Ir(4)	131.76(7)	Ir(2)−Fe(1)−Ir(3)	131.24(7)
Ir(2)−Fe(1)−Ir(4)	144.68(7)	Ir(3)−Fe(1)−Ir(4)	61.41(4)
S(1)−Fe(1)−S(2)	94.2(1)	S(1)−Fe(1)−S(3)	128.2(2)
S(1)−Fe(1)−S(4)	107.9(1)	S(2)−Fe(1)−S(3)	108.5(1)
S(2)−Fe(1)−S(4)	127.7(1)	S(3)−Fe(1)−S(4)	94.1(1)

Synthesis and X-ray Structures of Dicationic Pentanuclear Bow-Tie Clusters $[(Cp^*Ir)_2(\mu_3\text{-}S)_2M(\mu_3\text{-}S)_2(IrCp^*)_2]^{2+}$ (M = Fe, Co, Ni). On treatment with $NaBPh_4$ at 50 °C, cluster **3** was unexpectedly converted into the Ir_4Fe pentanuclear cluster $[(Cp^*Ir)_2(\mu_3\text{-}S)_2Fe(\mu_3\text{-}S)_2(IrCp^*)_2]^{2+}$ (**5**), which was isolated as a dark brown crystalline compound with the formula of $\mathbf{5}[BPh_4]_2\cdot CH_2Cl_2$ by recrystallization from CH_2Cl_2 (eq 2). In contrast, cluster **4** showed low reactivity toward $NaBPh_4$, and the rhodium analogue of **5** could not be obtained under similar conditions.

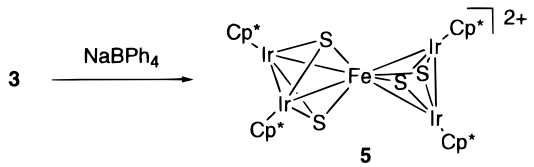

(2)

The molecular structure of $\mathbf{5}[BPh_4]_2\cdot CH_2Cl_2$ was crystallographically determined. The ORTEP drawing of the cation **5** is shown in Figure 2a, and selected bond distances and angles are listed in Table 2. The pentanuclear cluster core of **5** displays a typical bow-tie structure, where the two Ir_2Fe triangles share the central iron atom. The Ir−Ir contacts (2.7877(8), 2.7736(8) Å)[21] and Ir−Fe contacts (2.700(2)−2.727(2) Å)[21c−e,22] are all diagnostic of metal−metal single bonds and congruent with the 78e$^-$ structure. Each of the Ir_2Fe triangular fragments is capped by two μ_3-S ligands symmetrically from both sides, and the dihedral angle between the two Ir_2Fe planes is 73.4°. The Ir−S bond distances (av 2.277 Å) are similar to those found in **3** (av 2.297 Å), while the Fe−S bond distances (av 2.165 Å) are significantly shorter than those in **3** (av 2.338 Å). It should also be mentioned that cluster **5** is diamagnetic and shows a Cp* signal at δ 2.37 as a singlet in the ^{1}H NMR.

In contrast, complex **1** reacted with $CoCl_2$ at room temperature to afford directly the pentanuclear cluster $[(Cp^*Ir)_2(\mu_3\text{-}S)_2Co(\mu_3\text{-}S)_2(IrCp^*)_2]^{2+}$ (**6**). In the case of $NiCl_2\cdot 6H_2O$, a higher reaction temperature (50 °C) was required to obtain the pentanuclear cluster $[(Cp^*Ir)_2(\mu_3\text{-}S)_2Ni(\mu_3\text{-}S)_2(IrCp^*)_2]^{2+}$ (**7**) from a similar reaction (Scheme 1). Formation of HCl during

Scheme 1

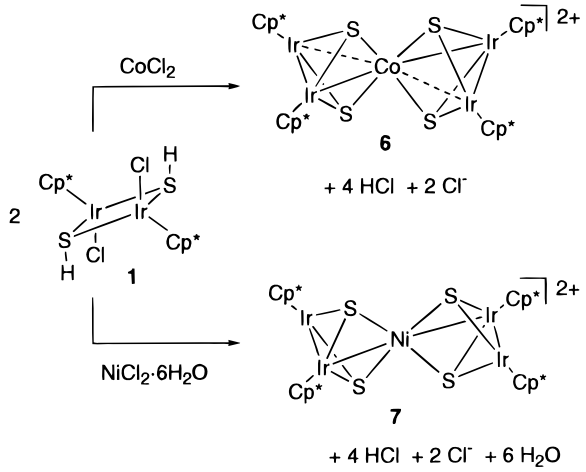

Table 3. Selected Interatomic Distances and Angles in $\mathbf{6}[CoCl_3(NCCH_3)]_2$

Bond Distances (Å)			
Ir(1)−Ir(2)	2.833(1)	Ir(1)−Co(1)	2.746(1)
Ir(2)−Co(1)	2.849(1)	Ir(1)−S(1)	2.286(5)
Ir(1)−S(2)	2.287(5)	Ir(2)−S(1)	2.284(4)
Ir(2)−S(2)	2.298(5)	Co(1)−S(1)	2.183(5)
Co(1)−S(2)	2.166(6)		
Bond Angles (deg)			
Ir(2)−Ir(1)−Co(1)	61.39(3)	Ir(1)−Ir(2)−Co(1)	57.79(3)
Ir(1)−Co(1)−Ir(2)	60.81(2)	Ir(1)−Co(1)−Ir(1*)	153.2(1)
Ir(1)−Co(1)−Ir(2*)	125.29(2)	Ir(2)−Co(1)−Ir(2*)	157.6(1)
S(1)−Co(1)−S(2)	91.5(2)	S(1)−Co(1)−S(1*)	98.6(3)
S(1)−Co(1)−S(2*)	144.6(2)	S(2)−Co(1)−S(2*)	99.6(3)

the reactions was confirmed in each case by isolation of $HNEt_3$-Cl from the reaction mixture. Cluster **7** was also isolated from the reaction of **1** with $Ni(cod)_2$ at room temperature (eq 3). In

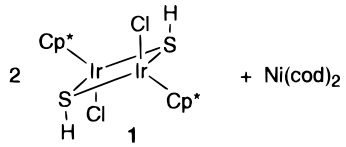

$\longrightarrow$ **7** + H_2 + 2 HCl + 2 Cl$^-$ + 2 cod (3)

this reaction, the starting Ni(0) was formally oxidized to Ni(II), and in agreement with this, evolution of H_2 (63% yield) was observed. In an attempt to synthesize analogous rhodium clusters, the reaction of complex **2** with $CoCl_2$ was examined, but the only product characterized was $[(Cp^*Rh)_3(\mu_3\text{-}S)_2][Co_2(\mu_2\text{-}Cl)_2Cl_4]\cdot MeCN$, the dicationic Rh_3S_2 core of which has recently been found in $[(Cp^*Rh)_3(\mu_3\text{-}S)_2][BF_4]_2$.[25]

Crystal structures of $\mathbf{6}[CoCl_3(NCMe)]_2$ and $\mathbf{7}[NiCl_4]\cdot CH_2Cl_2$ were determined by X-ray diffraction study. The ORTEP views are given in Figure 2b,c, and selected bond distances and angles are listed in Tables 3 and 4. Both the 79e$^-$ Ir_4Co cluster **6** and the 80e$^-$ Ir_4Ni cluster **7** have the pentanuclear bow-tie type core capped by four μ_3-S ligands, but the metrical parameters found for the metal−metal contacts in **6** and **7** are significantly different from those of the 78e$^-$ Ir_4Fe analogue **5**. The Ir_4Co cluster **6** has a crystallographic C_2 axis on which the central cobalt atom is located, and only one of the Ir_2Co triangular fragments is independent. The Ir_2Co framework is

(23) The ^{1}H NMR spectrum of the starting diiridium complex **1** in C_6D_6 displayed the Cp* signals at δ 1.30, 1.41, and 1.53 (two isomers). See ref 11.

(24) (a) Herrmann, W. A.; Barnes, C. E.; Zahn, T.; Ziegler, M. L. *Organometallics* **1985**, *4*, 172. (b) Barnes, C. E.; Dial, M. R.; Orvis, J. A.; Staley, D. L.; Rheingold, A. L. *Organometallics* **1990**, *9*, 1021.

(25) Nishioka, T.; Isobe, K. *Chem. Lett.* **1994**, 1661.

Table 4. Selected Interatomic Distances and Angles in **7**[$NiCl_4$]·CH_2Cl_2

Bond Distances (Å)			
Ir(1)−Ir(2)	2.837(1)	Ir(3)−Ir(4)	2.856(1)
Ir(1)−Ni(1)	2.700(3)	Ir(2)···Ni(1)	3.124(3)
Ir(3)−Ni(1)	2.683(3)	Ir(4)···Ni(1)	3.150(3)
Ir(1)−S(1)	2.290(5)	Ir(1)−S(2)	2.293(5)
Ir(2)−S(1)	2.287(5)	Ir(2)−S(2)	2.300(5)
Ir(3)−S(3)	2.293(5)	Ir(3)−S(4)	2.294(4)
Ir(4)−S(3)	2.300(5)	Ir(4)−S(4)	2.282(5)
Ni(1)−S(1)	2.234(6)	Ni(1)−S(2)	2.214(5)
Ni(1)−S(3)	2.205(5)	Ni(1)−S(4)	2.234(5)

Bond Angles (deg)			
Ir(2)−Ir(1)−Ni(1)	68.66(6)	Ir(4)−Ir(3)−Ni(1)	69.25(6)
Ir(1)−Ni(1)−Ir(3)	165.5(1)	S(1)−Ni(1)−S(2)	86.7(2)
S(1)−Ni(1)−S(3)	164.4(2)	S(1)−Ni(1)−S(4)	96.6(2)
S(2)−Ni(1)−S(3)	95.4(2)	S(2)−Ni(1)−S(4)	162.4(2)
S(3)−Ni(1)−S(4)	86.1(2)		

considerably unsymmetrical. The Ir(1)−Co(1) bond distance (2.746(1) Å) may be viewed as a metal−metal single bond, although it is somewhat longer than common Ir−Co single bond distances (2.47−2.67 Å).[26] In contrast, the Ir(2)−Co(1) contact (2.849(1) Å) is considerably elongated. The Ir(1)−Ir(2) bond (2.833(1) Å) is only slightly longer in comparison with the values found in cluster **5**. Thus, only two of the six metal−metal bonds in the bow-tie core are highly deformed by the substitution of cobalt for the central iron atom. The dihedral angle between the Ir_2Co planes is 49.9°.[27] The metal−S bond distances (Ir−S, av 2.289 Å; Co−S, av 2.175 Å) are similar to those in **5**.

In the Ir_4Ni cluster **7**, which is a rare example of Ir−Ni mixed metal clusters, further deformation of the core structure is observed. Two of the Ir−Ni bond distances (2.700(3), 2.683(3) Å) are indicative of metal−metal single bonds.[28] However, the other two Ir−Ni separations (3.150(3), 3.124(3) Å) are long, showing that there is no, or very weak, if any, bonding interaction between the Ni(1) and Ir(2) or Ir(4) atoms. Thus, the Ir_4Ni moiety has a Z-shaped core with four metal−metal bonds, in contrast to the metallospirane core with six metal−metal bonds found in **5** and **6**. Despite the considerable metrical variation in the Ir−Ni bonds, the Ir−Ir (2.837(1), 2.856(1) Å), Ir−S (av 2.292 Å), and Ni−S (av 2.222 Å) bonds exhibit only marginal elongation in comparison to the corresponding values found in **5** and **6**. The two Ir_2Ni planes are twisted with the torsion angle of 24.3°. If the Ir−Ni interactions are ignored, the geometry around the nickel atom is distorted square planar with four sulfido ligands.

Electrochemical Properties of Clusters 5−7 and Structures of Their One-Electron Reduction Products. The series of clusters **5**−**7** have the bow-tie Ir_4M core with four μ_3-S ligands as well as the cluster net charge of 2+ in common. Therefore they are expected to provide an excellent system for investigation of effects of central heterometal atoms in the Ir_4M bow-tie clusters on their physicochemical, especially electrochemical properties. Very recently, Holm and co-workers have reported the electrochemistry of heterobimetallic cuboidal MFe_3S_4 clusters and discussed the influence of the heterometals on the cluster redox potentials.[29] This work prompted us to compare the electrochemical effects of variant heterometals in the two series of clusters with different core structures.

Table 5. Redox Potentials (V, vs SCE) and Peak-to-Peak Separation (mV) for the Redox Changes Exhibited by **5**[BPh_4]$_2$, **6**[BPh_4]$_2$, and **7**[BPh_4]$_2$[a]

complex	$E_{1/2}^{+,0}$ (ΔE_p)	$E_{1/2}^{2+,+}$ (ΔE_p)	$E_{1/2}^{3+,2+}$ (ΔE_p)
5·[BPh_4]$_2$	−1.34 (135)	−0.43 (140)	0.98[b](150)
6·[BPh_4]$_2$	−1.23 (140)	−0.37 (130)	0.59 (100)
7·[BPh_4]$_2$	−1.04 (175)	−0.25 (100)	*c*

[a] In CH_2Cl_2-0.1 M [Bu^n_4N][BF_4], scan speed, 200 mVs^{-1}. [b] Quasireversible. [c] Oxidation waves (E_p) at 0.94, 1.08, and 1.28 V.

The redox properties of the dicationic bow-tie clusters **5**−**7** were investigated by cyclic voltammetry. The cyclic voltammograms of the tetraphenylborate salts of clusters, **5**[BPh_4]$_2$·CH_2Cl_2, **6**[BPh_4]$_2$·CH_2Cl_2, and **7**[BPh_4]$_2$·0.5CH_2Cl_2 were measured relative to SCE in CH_2Cl_2−0.1 M [Bu^n_4N][BF_4] at ambient temperature. The redox potentials obtained are summarized in Table 5. Each of clusters **5**−**7** showed two reversible reduction waves with good chemical reversibility based on the criterion that the i_p/i_a ratio is unity. In addition, **5** and **6** exhibit one quasireversible and reversible oxidation wave, respectively. The oxidation process of cluster **7** is complicated and irreversible; it showed three oxidation waves overlapping with each other. From the data listed in Table 5, the potential order Fe < Co < Ni is established for both the $[(Cp^*Ir)_2(\mu_3\text{-}S)_2M(\mu_3\text{-}S)_2(IrCp^*)_2]^{2+,+}$ and $[(Cp^*Ir)_2(\mu_3\text{-}S)_2M(\mu_3\text{-}S)_2(IrCp^*)_2]^{+,0}$ couples. Since clusters **5**−**7** have the common coordination structure and cluster net charge, this order is regarded to represent the intrinsic effect of the central heterometal on the redox behavior of the Ir_4M clusters. This point is further supported by the molecular structures of the one-electron reduction products $[(Cp^*Ir)_2(\mu_3\text{-}S)_2M(\mu_3\text{-}S)_2(IrCp^*)_2]^+$ (vide infra), which indicate that the electron added to each dicationic cluster is accommodated in an Ir−M antibonding orbital. It should be pointed out that the potential order obtained here is consistent with the standard aqueous electrode potentials ($E°$) for the electrode reaction $M^{2+} + 2e^- = M$ (M = Fe, −0.440 V; Co, −0.277 V; Ni, −0.250 V).[30] We suppose that in the present system the relative susceptibility of the M^{n+} ions to reduction is directly reflected in the potential order of the clusters. Furthermore, the potential order is in full agreement with that reported for the cuboidal MFe_3S_4 clusters by Holm et al.[29] It is of great interest that the two different cluster systems exhibit similar heterometal effects on the redox potentials.

To obtain further insight into the structures of the electrochemically reduced species, chemical reduction of clusters **5**−**7** was investigated. Indeed, reactions of **5**[BPh_4]$_2$, **6**[BPh_4]$_2$, and **7**[BPh_4]$_2$ with 1−2 equiv of Cp_2Co in THF led to isolation of the one-electron reduction products $[(Cp^*Ir)_2(\mu_3\text{-}S)_2M(\mu_3\text{-}S)_2(IrCp^*)_2]^+$ (**8**, M = Fe; **9**, M = Co; **10**, M = Ni) in good to moderate yields (Scheme 2). These clusters **8**[BPh_4], **9**[BPh_4], and **10**[BPh_4] were isolated as paramagnetic crystals, each of which was unambiguously characterized by X-ray diffraction analysis. The ORTEP views are given in Figure 2d−f, and selected bond distances and angles are summarized in Tables 6−8.

(26) (a) Hörlein, R.; Herrmann, W. A.; Barnes, C. E.; Weber, C.; Krüger, C.; Ziegler, M. L.; Zahn, T. *J. Organomet. Chem.* **1987**, *321*, 257. (b) Livotto, F. S.; Vargas, M. D.; Grepioni, F.; Braga, D. *J. Organomet. Chem.* **1993**, *452*, 197.

(27) This type of distortion from tetrahedral or planar geometry has been found in a few bow-tie clusters, but the reason has not been discussed (see refs 18c and 20c).

(28) (a) Pergola, R. D.; Garlaschelli, L.; Demartin, F.; Manassero, M.; Masciocchi, N.; Longoni, G. *J. Chem. Soc., Dalton Trans.* **1988**, 201. (b) Ceriotti, A.; Pergola, R. D.; Garlaschelli, L.; Manassero, M.; Masciocchi, N.; Sansoni, M. *J. Chem. Soc., Dalton Trans.* **1991**, 2357.

(29) Zhou, J.; Raebiger, J. W.; Crawford, C. A.; Holm, R. H. *J. Am. Chem. Soc.* **1997**, *119*, 6242.

(30) (a) In *Encyclopedia of Inorganic Chemistry*; King, R. B., Ed.; Wiley: Chichester, 1994. (b) The second ionization potentials may provide another guide to intrinsic potential orders of these metals; they are indeed in the order Fe (1.561 MJ mol^{-1}) < Co (1.646 MJ mol^{-1}) < Ni (1.753 MJ mol^{-1}); see ref 30a.

Scheme 2

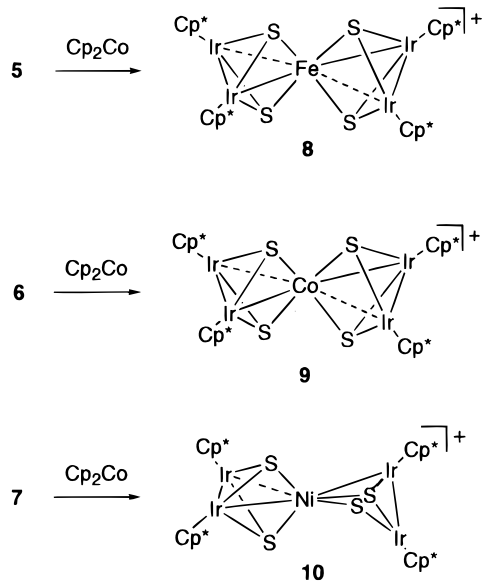

Table 6. Selected Interatomic Distances and Angles in **8**[BPh_4]

Bond Distances (Å)			
Ir(1)−Ir(2)	2.7509(7)	Ir(3)−Ir(4)	2.7910(9)
Ir(1)−Fe(1)	2.769(2)	Ir(2)−Fe(1)	2.863(2)
Ir(3)−Fe(1)	2.747(2)	Ir(4)−Fe(1)	2.861(2)
Ir(1)−S(1)	2.303(3)	Ir(1)−S(2)	2.294(3)
Ir(2)−S(1)	2.291(4)	Ir(2)−S(2)	2.305(3)
Ir(3)−S(3)	2.299(3)	Ir(3)−S(4)	2.306(3)
Ir(4)−S(3)	2.323(3)	Ir(4)−S(4)	2.287(3)
Fe(1)−S(1)	2.198(3)	Fe(1)−S(2)	2.183(4)
Fe(1)−S(3)	2.194(3)	Fe(1)−S(4)	2.201(4)
Bond Angles (deg)			
Ir(2)−Ir(1)−Fe(1)	62.50(4)	Ir(1)−Ir(2)−Fe(1)	59.06(4)
Ir(4)−Ir(3)−Fe(1)	62.21(4)	Ir(3)−Ir(4)−Fe(1)	58.14(4)
Ir(1)−Fe(1)−Ir(2)	58.45(4)	Ir(1)−Fe(1)−Ir(3)	150.47(7)
Ir(1)−Fe(1)−Ir(4)	128.40(6)	Ir(2)−Fe(1)−Ir(3)	129.13(6)
Ir(2)−Fe(1)−Ir(4)	154.63(7)	Ir(3)−Fe(1)−Ir(4)	59.65(4)
S(1)−Fe(1)−S(2)	92.4(1)	S(1)−Fe(1)−S(3)	139.0(1)
S(1)−Fe(1)−S(4)	101.9(1)	S(2)−Fe(1)−S(3)	101.9(1)
S(2)−Fe(1)−S(4)	138.3(1)	S(3)−Fe(1)−S(4)	92.6(1)

Table 7. Selected Interatomic Distances and Angles in **9**[BPh_4]

Bond Distances (Å)			
Ir(1)−Ir(2)	2.815(1)	Ir(3)−Ir(4)	2.7719(7)
Ir(1)−Co(1)	2.777(1)	Ir(2)−Co(1)	2.884(2)
Ir(3)−Co(1)	2.786(1)	Ir(4)−Co(1)	2.891(1)
Ir(1)−S(1)	2.289(3)	Ir(1)−S(2)	2.295(3)
Ir(2)−S(1)	2.305(3)	Ir(2)−S(2)	2.284(3)
Ir(3)−S(3)	2.299(3)	Ir(3)−S(4)	2.298(3)
Ir(4)−S(3)	2.299(3)	Ir(4)−S(4)	2.296(3)
Co(1)−S(1)	2.247(3)	Co(1)−S(2)	2.246(3)
Co(1)−S(3)	2.228(3)	Co(1)−S(4)	2.253(3)
Bond Angles (deg)			
Ir(2)−Ir(1)−Co(1)	62.10(3)	Ir(1)−Ir(2)−Co(1)	58.30(3)
Ir(4)−Ir(3)−Co(1)	62.68(3)	Ir(3)−Ir(4)−Co(1)	58.91(3)
Ir(1)−Co(1)−Ir(2)	59.60(3)	Ir(1)−Co(1)−Ir(3)	147.44(5)
Ir(1)−Co(1)−Ir(4)	131.12(5)	Ir(2)−Co(1)−Ir(3)	130.41(5)
Ir(2)−Co(1)−Ir(4)	151.47(5)	Ir(3)−Co(1)−Ir(4)	58.42(3)
S(1)−Co(1)−S(2)	90.01(9)	S(1)−Co(1)−S(3)	106.5(1)
S(1)−Co(1)−S(4)	135.4(1)	S(2)−Co(1)−S(3)	134.9(1)
S(2)−Co(1)−S(4)	106.6(1)	S(3)−Co(1)−S(4)	90.7(1)

In all of these three cases, the bow-tie core capped by four μ_3-S ligands is maintained. The one-electron reduction affects the Ir−Ir (**8**, av 2.7710; **9**, av 2.7935; **10**, av 2.8103 Å), Ir−S (**8**, av 2.301; **9**, av 2.296; **10**, av 2.292 Å), and M−S (**8**, av 2.194; **9**, av 2.244; **10**, av 2.261 Å) bond distances in these clusters only to a minor extent. However, the Ir−M bond distances display remarkable changes reflecting profound effects of the increase in the valence electrons. In the 79e$^-$ cluster **8**, two types of Ir−Fe bonds are observed. The shorter Ir(1)−Fe(1) (2.769(2) Å) and Ir(3)−Fe(1) (2.747(2) Å) bonds are consistent with metal−metal single bonds,[21c−e,22] while the longer Ir(2)−Fe(1) (2.863(2) Å) and Ir(4)−Fe(1) (2.861(2) Å) contacts indicate that the bond order of these interactions is lower than unity. It should be noted that the metal−metal separations found in **8** are closely related to those found in the other 79e$^-$ cluster **6**, except that the Ir−Ir bonds in **6** are shorter by 0.04−0.08 Å. Similarly, in the 80e$^-$ cluster **9**, the Ir−Co bonds include two shorter metal−metal bonds (Ir(1)−Co(1), 2.777(1) Å; Ir(3)−Co(1), 2.786(1) Å) and two longer contacts (Ir(2)−Co(1), 2.884(1) Å; Ir(4)−Co(1), 2.891(1) Å). Interestingly, each of these bonds is only slightly (0.04 Å) longer than the corresponding short and long Ir−Co bonds found in **6**, and the perturbation caused by the one-electron reduction is exceptionally small.

Table 8. Selected Interatomic Distances and Angles in **10**[BPh_4]

Bond Distances (Å)			
Ir(1)−Ir(2)	2.8199(7)	Ir(3)−Ir(4)	2.8007(8)
Ir(1)−Ni(1)	2.686(1)	Ir(2)···Ni(1)	2.941(2)
Ir(3)−Ni(1)	2.596(1)	Ir(4)···Ni(1)	3.281(2)
Ir(1)−S(1)	2.295(3)	Ir(1)−S(2)	2.291(3)
Ir(2)−S(1)	2.281(3)	Ir(2)−S(2)	2.303(3)
Ir(3)−S(3)	2.306(3)	Ir(3)−S(4)	2.297(3)
Ir(4)−S(3)	2.288(3)	Ir(4)−S(4)	2.274(3)
Ni(1)−S(1)	2.261(3)	Ni(1)−S(2)	2.205(3)
Ni(1)−S(3)	2.274(3)	Ni(1)−S(4)	2.305(4)
Bond Angles (deg)			
Ir(2)−Ir(1)−Ni(1)	64.51(4)	Ir(1)−Ir(2)−Ni(1)	55.54(3)
Ir(4)−Ir(3)−Ni(1)	74.78(4)	Ir(1)−Ni(1)−Ir(2)	59.95(3)
Ir(1)−Ni(1)−Ir(3)	142.20(6)	Ir(2)−Ni(1)−Ir(3)	135.68(6)
S(1)−Ni(1)−S(2)	90.3(1)	S(1)−Ni(1)−S(3)	139.6(1)
S(1)−Ni(1)−S(4)	116.5(1)	S(2)−Ni(1)−S(3)	106.3(1)
S(2)−Ni(1)−S(4)	124.9(1)	S(3)−Ni(1)−S(4)	84.0(1)

The 81e$^-$ cluster **10**, the two Ir−Ni single bonds (Ir(1)−Ni(1), 2.686(1) Å; Ir(3)−Ni(1), 2.596(1) Å) are retained, and in addition, a weak Ir−Ni interaction exists between the Ir(2) and Ni(1) atoms (2.941(2) Å) which is not seen in the parent dication **7**. The Ir(4)−Ni(1) separation (3.281(2) Å) is long enough to be considered as nonbonding. Therefore, one-electron reduction of **7** induced the formation of a new weak metal−metal bond. Another outstanding structural difference between **10** and **7** is found in the dihedral angle between the Ir_2Ni planes. The dihedral angles of 71.3° found in **10** and 24.3° in **7** indicate that the geometry around the Ni(1) atom is deformed from distorted square planar to distorted tetrahedral by reduction.

Structural and Bonding Analysis of 78/79/80/81-Electron Clusters $[(Cp^*Ir)_2(\mu_3\text{-}S)_2M(\mu_3\text{-}S)_2(IrCp^*)_2]^{n+}$ (M = Fe, Co, Ni; n = 1, 2). As described above, the six pentanuclear clusters synthesized in this study have the common bow-tie structure with four μ_3-S ligands. In all cases, the Ir−Ir distances are diagnostic of a single metal−metal bond, while the interaction between the iridium and the central heterometal atom varies significantly with the oxidation state of the cluster core and the nature of the heterometal. Two distinct types of Ir−M bonds are observed besides the nonbonding Ir−M separations found in the Ir_4Ni clusters. The class of shorter bond distances (2.60−2.79 Å) fall in or somewhat exceed the range of the known Ir−M single bond distances, and the group of longer bond distances (2.85−2.94 Å) correspond to weak bonding interactions.

The 78e$^-$ cluster **5** has, as expected from the electron-counting, four Fe−Ir single bonds. The dihedral angle of 73.4°

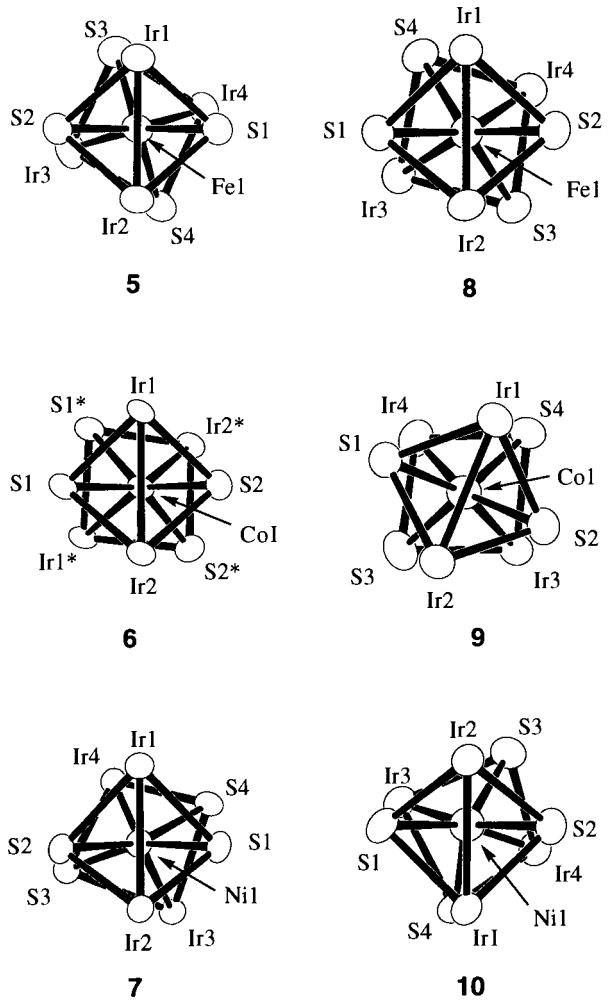

Figure 3. Side views of the cluster cores in **5**−**10** along the Ir_2−M−Ir_2 axis.

between the Ir_2Fe planes implies that the iron atom is situated in the center of a distorted tetrahedron composed of the four sulfido ligands (Figure 3). Extended Hückel molecular orbital calculations for the hypothetical $[(CpIr)_2(\mu_3\text{-}S)_2Fe(\mu_3\text{-}S)_2(IrCp)_2]^{2+}$ ion with D_2-idealized structures indicate that the total energy of this ion decreases with increasing the dihedral angle (θ) between the two Ir_2Fe planes from 0 to 60°, but with higher θ values, it is essentially independent of the θ values (Figure 4a). We consider that the deviation of the dihedral angle from 90° (D_{2d} symmetry) is ascribed mainly to the steric congestion between the Cp* groups on each Ir_2Fe fragment and the μ_3-S ligands on the other Ir_2Fe moiety. In fact, the closest contact between the μ_3-S ligand and the Cp* methyl group in **5** is 3.68(2) Å (S(2)···C(28), Figure 2a), which is shorter than the sum of each van der Waals radius of a sulfur atom (1.85 Å) and a methyl group (2.0 Å).[31]

The substitution of the central iron atom in **5** with a cobalt atom and the one-electron reduction of **5** form the 79e$^-$ clusters **6** and **8**, respectively. Both clusters exhibit closely related structures to each other, in which only two of the four Ir−M bonds are significantly lengthened. It appears that the "extra" electron is added to an Ir−M antibonding orbital to decrease the Ir−M bond order. To make this point clear, molecular orbitals for the $[(CpIr)_2(\mu_3\text{-}S)_2Fe(\mu_3\text{-}S)_2(IrCp)_2]^{2+}$ ion with idealized D_{2d} symmetry modeled from **5** and those with a C_2 structure ($\theta = 90°$) modeled from compound **8** are compared to each other (Figure 5). For both the D_{2d} and C_2 structures, the LUMO is antibonding and nonbonding with respect to the Ir−Fe and Ir−Ir bonds, respectively. The unsymmetric elongation of the Ir−Fe bonds, which lowers the symmetry of the cluster core from apparent D_{2d} to C_2, is considered to be the result of the second-order Jahn−Teller effect.[32] In fact, the molecular orbital diagram for $[(CpIr)_2(\mu_3\text{-}S)_2Fe(\mu_3\text{-}S)_2(IrCp)_2]^{2+}$ ion with D_{2d} symmetry indicates that occupation of the LUMO with one electron should give an A_1 ground state which couples to an excited state of E symmetry. Since the direct product $A_1 \times E$ is E, the second-order Jahn−Teller distortion is expected to take the form of e vibration, which leads to the distortion actually observed in **8**, namely, the elongation of one of the Ir−Fe bonds in each $FeIr_2$ triangular fragment. Upon such deformation, the LUMO in the D_{2d} structure ($2a_1$) is mixed with the second LUMO 1e (maybe also 2e) and stabilized. It is worth mentioning that the resultant LUMO in the C_2 structure (1a), where the odd electron in **8** would be placed, is strongly antibonding with respect to the two elongated Fe−Ir bonds.

Figure 4b depicts the calculated total energy for the hypothetical $[(CpIr)_2(\mu_3\text{-}S)_2Fe(\mu_3\text{-}S)_2(IrCp)_2]^{+}$ ion as a function of the dihedral angle (θ) between the two Ir_2Fe planes. In sharp contrast to the corresponding dication (Figure 4a), this monocationic cluster has two stable conformations with the θ values of 45 and 135°, and the conformation with the θ value of 90° (the S_4 coordination geometry around the iron is elongated tetrahedral) is unstable. In the conformer of the corresponding Cp* cluster **8** with the θ value of 135°, the Cp* ligands on the Ir(1) and Ir(3) atoms are considered to be brought close together so that the steric congestion between the Cp* methyl groups makes this conformation much less stable. Therefore, the θ value of approximately 45° is expected for cluster **8**. Actually, the crystallographically observed dihedral angle between the Ir_2Fe planes in **8** is 57.6°, which is congruent with the prediction from the calculation.[27]

Similar calculation results were also obtained for the 79e$^-$ cobalt cluster **6**, which has the crystallographically determined dihedral angle of 49.9° between the two Ir_2Co planes. The molecular orbital diagram for $[(CpIr)_2(\mu_3\text{-}S)_2Co(\mu_3\text{-}S)_2(IrCp)_2]^{2+}$ ion also shows that the HOMO 1a orbital is again antibonding with respect to two of the Ir−Co bonds as in the case of the isoelectronic iron cluster $[(CpIr)_2(\mu_3\text{-}S)_2Fe(\mu_3\text{-}S)_2(IrCp)_2]^{+}$ (Figure 6).

The two 80e$^-$ clusters **7** and **9** showed considerably different core structures from each other. In the cobalt cluster **9**, the six metal−metal bonds are retained. The comparison between the structures of the cobalt clusters **6** and **9** reveals that the one-electron reduction of **6** lengthens the four Ir−Co bonds slightly (0.04 Å) and almost equally. The ^{1}H NMR spectrum of **9**[BPh_4] in CD_2Cl_2 at 20 °C exhibited the Cp* methyl singlet at δ −12.67, which indicates the diradical character of **9**. Variable temperature ^{1}H NMR measurement displayed a linear correlation between the isotropic shift and inverse temperature over the temperature range of −60 to 20 °C, although extrapolation to infinite temperature yielded a paramagnetically derived intercept (δ 5.33). The magnetic susceptibility of **9**[BPh_4] in the solid state at 18 °C ($\mu_{eff} = 2.66\ \mu_B$) is also consistent with these observations. The slight elongation of the metal−metal bonds and the paramagnetic nature of **9** would be explained as a result

(31) Pauling, L. In *The Nature of the Chemical Bond*, 3rd ed.; Cornell University Press: Ithaca, NY, 1960.

(32) (a) Albright, T. A.; Burdett, J. K.; Whangbo, M. H. In *Orbital Interactions in Chemistry*; Wiley: New York, 1985; p 95. (b) Cotton, F. A.; Fang, A. *J. Am. Chem. Soc.* **1982**, *104*, 113.

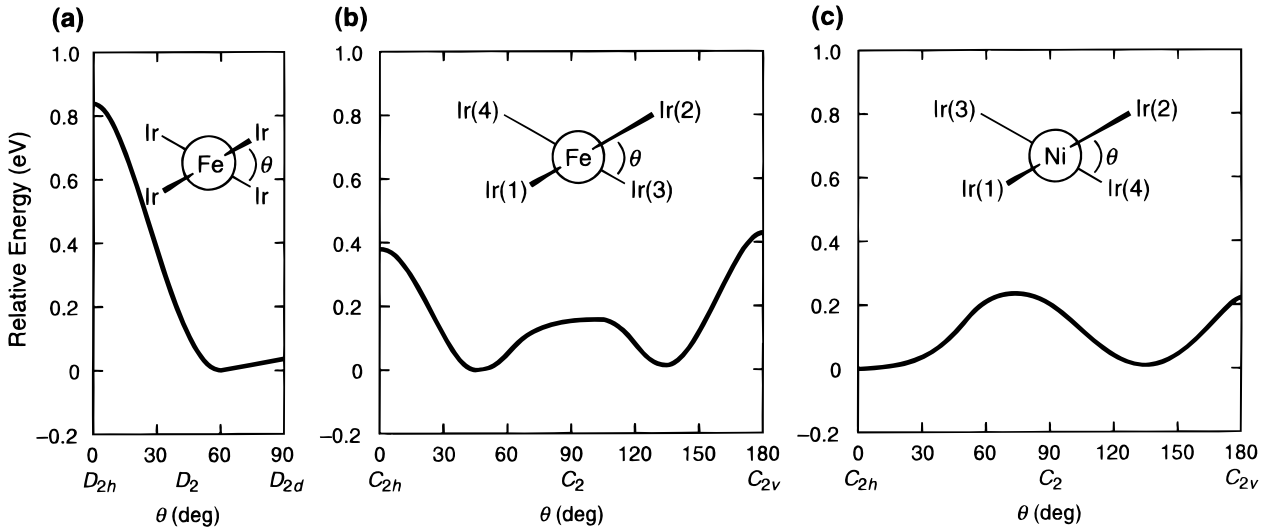

Figure 4. Angular dependence of the total energies for D_2-idealized $[(CpIr)_2(\mu_3\text{-}S)_2Fe(\mu_3\text{-}S)_2(IrCp)_2]^{2+}$ (a), C_2-idealized $[(CpIr)_2(\mu_3\text{-}S)_2Fe(\mu_3\text{-}S)_2(IrCp)_2]^{+}$ (b), and C_2-idealized $[(CpIr)_2(\mu_3\text{-}S)_2Ni(\mu_3\text{-}S)_2(IrCp)_2]^{2+}$ (c) ions.

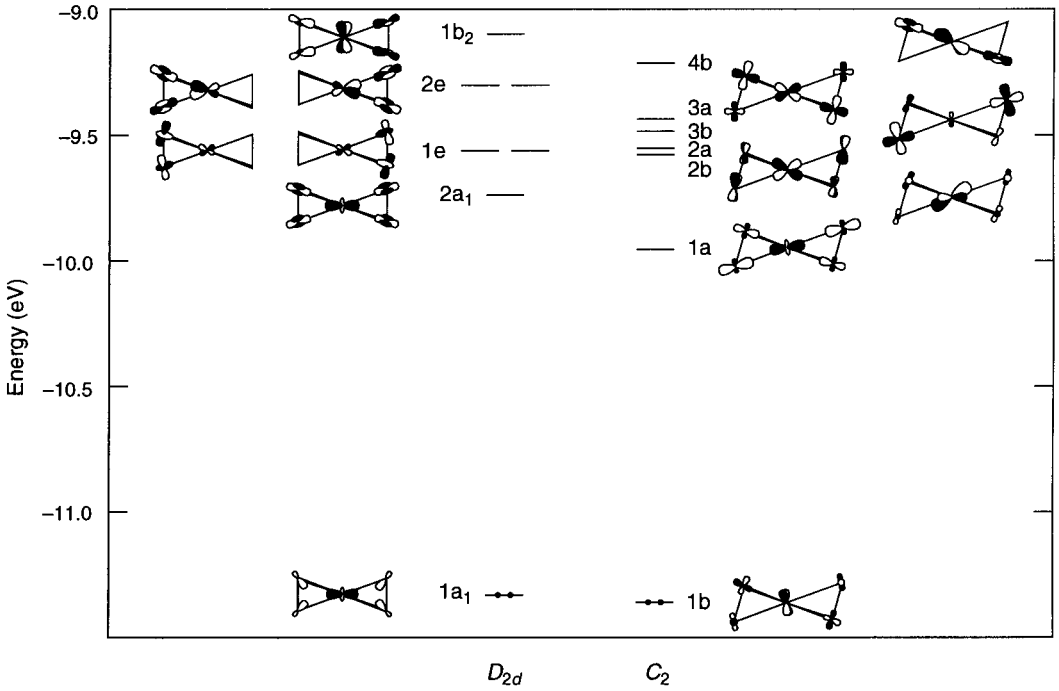

Figure 5. Orbital diagrams for $[(CpIr)_2(\mu_3\text{-}S)_2Fe(\mu_3\text{-}S)_2(IrCp)_2]^{2+}$ ion with D_{2d} symmetry (left) and C_2 symmetry (right), where the dihedral angle between the two Ir_2Fe planes is 90°.

of the accommodation of the added electron in the weakly metal−metal antibonding orbital 2b (Figure 6); occupation of the 1a and 2b orbitals by two unpaired electrons leads to a high-spin state for cluster **9**.

In contrast, the nickel cluster **7** has a Z-shaped core with two Ir−Ir and two Ir−Ni bonds; two of the Ir−Ni contacts are nonbonding. The two Ir_2Ni planes intersect each other with the dihedral angle of 24.2°, and the coordination environment around the central nickel atom is distorted square planar. The deviation from the planarity may be accounted for by the steric repulsion between the Cp* methyl groups on the two Ir_2Ni fragments, which is most typically demonstrated by the very close contact of 3.32(3) Å between the C(10) and C(37) atoms (Figure 2c). Although the electron count requires five metal−metal bonds to satisfy the effective atomic number (EAN) of 18 electrons per a metal atom, group 10 metals in square planar complexes are known to have a high-lying atomic p_z orbital perpendicular to the coordination plane, so that the molecular orbitals derived from this atomic orbital do not often contribute to metal−metal bonding.[12] Obviously this is the case for cluster **7**.

Cluster **7**$[BPh_4]_2$ is paramagnetic in the solid state at 18 °C (μ_{eff} = 3.01 μ_B) and shows a very broad ^1H NMR signal at δ 0.47 in CD_2Cl_2 at 20 °C assignable to the Cp* groups. The molecular orbital diagram for the Cp analogue of **7**, $[(CpIr)_2(\mu_3\text{-}S)_2Ni(\mu_3\text{-}S)_2(IrCp)_2]^{2+}$ with an idealized C_{2h} symmetry, is depicted in Figure 7. The observed paramagnetic nature of **7** demands a high-spin state, and thus the two unpaired electrons seem to be accommodated in the $1a_g$ and $2b_u$ orbitals, although the energy gap between these orbitals is fairly large (1.14 eV). It should be pointed out that the $2a_g$ orbital, the LUMO in this electronic configuration, has a significant Ni 3d character, and the occupation of this orbital by an added electron would make all five 3d orbitals of the nickel atom available for bonding,

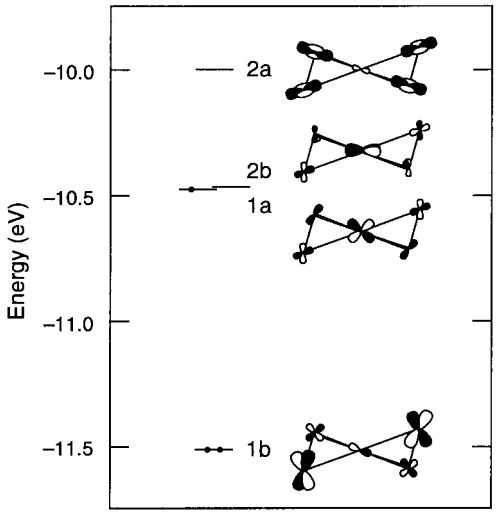

Figure 6. Orbital diagram for C_2-idealized $[(CpIr)_2(\mu_3\text{-}S)_2Co(\mu_3\text{-}S)_2(IrCp)_2]^{2+}$ ion with the dihedral angle of 90° between the two Ir_2Fe planes.

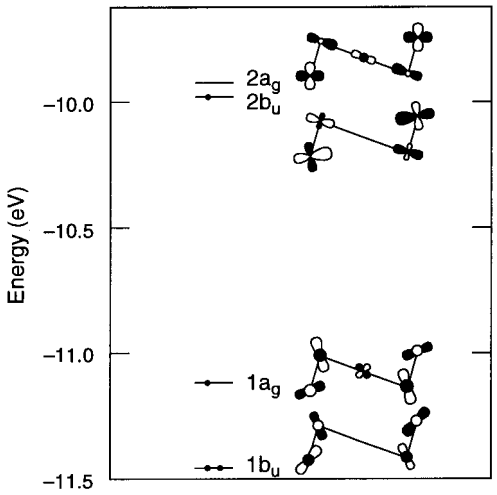

Figure 7. Orbital diagram for $[(CpIr)_2(\mu_3\text{-}S)_2Ni(\mu_3\text{-}S)_2(IrCp)_2]^{2+}$ ion with C_{2h} symmetry.

which may result in the tetrahedral geometry around the nickel atom in **10** rather than the square-planar structure observed in **7** (vide infra).

The effect of the dihedral angle between the two Ir_2Ni planes (θ) on the stability of the 80e$^-$ nickel cluster has also been investigated. Figure 4c depicts how the total energy of the C_2-idealized $[(CpIr)_2(\mu_3\text{-}S)_2Ni(\mu_3\text{-}S)_2(IrCp)_2]^{2+}$ changes depending upon the value of θ. The total energies were calculated on the assumption that the cluster conserves the high-spin state, that is, the two unpaired electrons remain to occupy the orbitals derived from the $1a_g$ and $2b_u$ in Figure 7. The cluster has two stable conformations with the θ value of 0° and 135°. However, the latter conformer is considered to be much less stable due to the steric congestion between the Cp* groups as described for cluster **8**, and this calculation result is again in good agreement with the observed structure of **7** (vide supra).

Finally, the electronic structure of the 81e$^-$ nickel cluster **10** is discussed. The molecular orbital diagram for $[(CpIr)_2(\mu_3\text{-}S)_2Ni(\mu_3\text{-}S)_2(IrCp)_2]^{2+}$ (Figure 7) indicates that the added electron would occupy the LUMO ($2a_g$), which has a close energy level to that of the HOMO and a considerable Ni 3d character. Occupation of this orbital would cause the change of the coordination geometry around the nickel atom from square-planar to tetrahedral (vide supra). This is exactly the case for cluster **10**. Figure 3 clearly shows a drastic change of the dihedral angle between the two Ir_2Ni planes (**7**, 24.22°; **10**: 71.33°) upon the one-electron reduction. Participation of all five Ni 3d orbitals in bonding also makes cluster **10** to obey the typical EAN rule: in agreement with the 81 valence electron count, cluster **10** exhibits two Ir−Ir and two Ir−Ni single bonds along with a weak Ir−Ni interaction, and the total number of metal−metal bonds amounts to 4.5.

In conclusion, a new series of pentanuclear bow-tie clusters $[(Cp^*Ir)_2(\mu_3\text{-}S)_2M(\mu_3\text{-}S)_2(IrCp^*)_2]^{n+}$ with 78−81 valence electrons have been prepared, and their structures and redox properties have been investigated. The potential order Fe < Co < Ni has been established for both the $[(Cp^*Ir)_2(\mu_3\text{-}S)_2M(\mu_3\text{-}S)_2(IrCp^*)_2]^{2+,+}$ and $[(Cp^*Ir)_2(\mu_3\text{-}S)_2M(\mu_3\text{-}S)_2(IrCp^*)_2]^{+,0}$ couples. The structures and bonding in the six cluster cores were explained in terms of the valence electron counts and molecular orbital calculations of the clusters. This is the first systematic study on 78−81e$^-$ bow-tie clusters, and provides important information about the structures of this class and related cluster compounds.

Experimental Section

General Consideration. All manipulations were carried out under an atmosphere of nitrogen by the use of Schlenk techniques. Solvents were dried by common procedures and degassed before use. Complexes **1** and **2** were prepared according to the literature methods.[11] $FeCl_2{\cdot}4H_2O$, $CoCl_2$, $NiCl_2{\cdot}6H_2O$, Cp_2Co, $NaBPh_4$, and other organic reagents were commercially obtained and used without further purification. ^{1}H NMR spectra were recorded on a JEOL EX-270 spectrometer. Electrochemical measurements were made with Hokuto Denko instrumentation (HA-501 potentiostat and HB-105 function generator) by using a glassy carbon working electrode; potentials were measured in CH_2Cl_2−0.1 M $[Bu^n{}_4N][BF_4]$ vs an SCE. Magnetic susceptibility measurements were performed with a Shimadzu magnetic balance MB-100 (Faraday method) at room temperature. Elemental analyses were done with a Perkin-Elmer 2400II CHN analyzer.

Synthesis of $[(Cp^*Ir)_2(\mu_3\text{-}S)_2FeCl_2]$ (3). To a suspension of **1** (129 mg, 0.163 mmol) in THF (8 mL) was added $FeCl_2{\cdot}4H_2O$ (65 mg, 0.327 mmol), and the mixture was stirred at room temperature for 15 h. The color of the suspension changed from yellow to green. The solvent was removed by filtration, and the residual solid was washed with ether and extracted with CH_2Cl_2. Addition of hexane to the concentrated CH_2Cl_2 solution afforded **3** (125 mg, 0.148 mmol, 91% yield) as dark green crystals. In a separate run using 0.136 mmol of **1**, the volatile products were collected from the crude reaction mixture by means of a cold trap and neutralized with NEt_3 to give $HNEt_3Cl$ (0.248 mmol, 91% yield, identified by ^{1}H NMR, IR, and elemental analysis), indicating the reaction was accompanied by the formation of two HCl molecules. ^{1}H NMR ($CDCl_3$, 25 °C): δ −30.86. Anal. Calcd for $C_{20}H_{30}Cl_2FeIr_2S_2$: C, 28.40; H, 3.58. Found: C, 28.37; H, 3.69. μ_{eff} = 5.22 μ_B.

Synthesis of $[(Cp^*Rh)_2(\mu_3\text{-}S)_2FeCl_2]$ (4). This complex was prepared from **2** by a similar procedure to that described for **3** and isolated in 41% yield as dark green crystals. ^{1}H NMR (δ, $CDCl_3$, 23 °C): −30.94. Anal. Calcd for $C_{20}H_{30}Cl_2FeRh_2S_2$: C, 36.01; H, 4.53. Found: C, 35.58; H, 4.39.

Synthesis of $[(Cp^*Ir)_2(\mu_3\text{-}S)_2Fe(\mu_3\text{-}S)_2(IrCp^*)_2][BPh_4]_2{\cdot}CH_2Cl_2$ ($5[BPh_4]_2{\cdot}CH_2Cl_2$). To a suspension of **3** (30 mg, 0.035 mmol) in THF (8 mL) was added $NaBPh_4$ (50 mg, 0.146 mmol), and the mixture was stirred at 50 °C for 15 h. The color of the suspension changed from green to dark red. The solvent was removed by filtration, and the residual solid was washed with ether and extracted with CH_2Cl_2. Addition of hexane to the concentrated CH_2Cl_2 solution afforded $5[BPh_4]_2{\cdot}CH_2Cl_2$ (30 mg, 0.014 mmol, 77% yield) as dark brown crystals. ^{1}H NMR (δ, acetone-d_6, 0 °C): 2.37 (s, 60 H, Cp*), 6.72 (t, J = 7.3 Hz, 8 H, *p*-H of BPh_4), 6.87 (t, J = 7.3 Hz, 16 H, *m*-H of BPh_4), 7.27 (br, 16 H, *o*-H of BPh_4). Anal. Calcd for $C_{89}H_{102}B_2Cl_2FeIr_4S_4$: C, 48.21; H, 4.64. Found: C, 48.31; H, 4.61.

Table 9. X-ray Crystallographic Data for **3**, **4**, **5**$[BPh_4]_2\cdot CH_2Cl_2$, and **6**$[CoCl_3(NCMe)]_2$

	3	**4**	**5**$[BPh_4]_2\cdot CH_2Cl_2$	**6**$[CoCl_3(NCMe)]_2$
empirical formula	$C_{20}H_{30}Cl_2FeIr_2S_2$	$C_{20}H_{30}Cl_2FeRh_2S_2$	$C_{89}H_{102}B_2Cl_2FeIr_4S_4$	$C_{44}H_{66}N_2Cl_6Co_3Ir_4S_4$
fw	845.77	667.14	2217.28	1909.66
cryst syst	monoclinic	monoclinic	triclinic	monoclinic
space group	*C*2/*c*	*C*2/*c*	$P\bar{1}$	*C*2/*c*
cryst size, mm	0.30 × 0.15 × 0.30	0.10 × 0.15 × 0.80	0.10 × 0.20 × 0.85	0.20 × 0.20 × 0.60
a, Å	33.543(5)	33.443(2)	16.899(2)	28.914(4)
b, Å	8.828(3)	8.832(3)	23.646(5)	8.516(3)
c, Å	17.482(2)	17.457(2)	11.400(2)	23.950(2)
α, deg			101.47(2)	
β, deg	109.44(2)	109.656(8)	102.12(1)	98.091(10)
γ, deg			76.00(1)	
V, Å^3	4881(1)	4855(1)	4268(1)	5838(2)
Z	8	8	2	4
D_{calc}, g cm^{-3}	2.301	1.825	1.725	2.172
μ(Mo Kα), cm^{-1}	118.87	23.25	65.99	103.85
no. of unique rflns	5995	5968	15031	7146
no. of rflns used [$I > 3\sigma(I)$]	3331	3436	9204	4247
R^a	0.066	0.041	0.048	0.070
$R_w{}^b$	0.047	0.027	0.037	0.052
GOF^c	2.62	1.99	1.87	2.82

^{a} $R = \sum||F_o| - |F_c||/\sum|F_o|$. ^{b} $R_w = [\sum w(|F_o| - |F_c|)^2/\sum wF_o^2]^{1/2}$, $w = 1/\sigma^2(F_o)$. ^{c} GOF $= [\sum w(|F_o| - |F_c|)^2/(N_{obs} - N_{params})]^{1/2}$.

Synthesis of [(Cp*Ir)$_2$(μ_3-S)$_2$Co(μ_3-S)$_2$(IrCp*)$_2$][CoCl$_3$(NCMe)]$_2$ (6[CoCl$_3$(NCMe)]$_2$). To a suspension of **1** (100 mg, 0.126 mmol) in THF (8 mL) was added $CoCl_2$ (25 mg, 0.193 mmol), and the mixture was stirred at room temperature for 18 h to give a dark brown suspension. The precipitate was collected by filtration, washed with ether, and dissolved in MeCN. Addition of THF and hexane to the concentrated MeCN solution afforded **6**$[CoCl_3(NCMe)]_2$ (90 mg, 0.047 mmol, 75% yield) as dark brown crystals. In a separate run, concomitant formation of HCl was confirmed by trapping it as $HNEt_3$-Cl (84% yield based on **1**). Anal. Calcd for $C_{44}H_{66}N_2Cl_6Co_3Ir_4S_4$: C, 27.67; H, 3.48; N, 1.47. Found: C, 27.49; H, 3.47; N, 1.24.

Synthesis of [(Cp*Ir)$_2$(μ_3-S)$_2$Co(μ_3-S)$_2$(IrCp*)$_2$][BPh$_4$]$_2\cdot$CH$_2$Cl$_2$ (6[BPh$_4$]$_2\cdot$CH$_2$Cl$_2$). To a solution of **6**$[CoCl_3(NCMe)]_2$ (117 mg, 0.061 mmol) in CH_2Cl_2 (8 mL) was added $NaBPh_4$ (172 mg, 0.502 mmol) in THF (8 mL), and the mixture was stirred at room temperature for 15 h. The solvent was removed in vacuo, and the residual solid was extracted with CH_2Cl_2. Addition of hexane to the concentrated CH_2-Cl_2 solution afforded **6**$[BPh_4]_2\cdot CH_2Cl_2$ (110 mg, 0.050 mmol, 81% yield) as dark brown crystals. Anal. Calcd for $C_{89}H_{102}B_2Cl_2CoIr_4S_4$: C, 48.14; H, 4.63. Found: C, 48.01; H, 4.52. $\mu_{eff} = 1.77\ \mu_B$.

Synthesis of [(Cp*Ir)$_2$(μ_3-S)$_2$Ni(μ_3-S)$_2$(IrCp*)$_2$][NiCl$_4$]$\cdot$CH$_2$Cl$_2$ (7[NiCl$_4$]$\cdot$CH$_2$Cl$_2$). To a suspension of **1** (94 mg, 0.119 mmol) in THF (8 mL) was added $Ni(cod)_2$ (39 mg, 0.142 mmol), and the mixture was stirred at room temperature for 72 h. GC analysis of the gas phase confirmed the evolution of H_2 gas in 63% yield. The solvent was removed by filtration, and the residual solid was washed with ether and extracted with MeCN. Addition of CH_2Cl_2 and hexane to the concentrated MeCN solution afforded **7**$[NiCl_4]\cdot CH_2Cl_2$ (48 mg, 0.027 mmol, 45% yield) as dark brown crystals. Anal. Calcd for $C_{41}H_{62}$-$Cl_6Ir_4Ni_2S_4$: C, 27.63; H, 3.51. Found: C, 27.61; H, 3.71.

In a separate run, complex **1** (112 mg, 0.141 mmol) and $NiCl_2\cdot 6H_2O$ (39 mg, 0.16 mmol) were allowed to react in THF (8 mL) at 50 °C for 84 h. The resulting brown precipitate was collected by filtration, washed with ether, and dissolved in MeCN. The MeCN solution was filtered and concentrated in vacuo, and the brown residue was dissolved in CH_2Cl_2. Addition of ether to the CH_2Cl_2 solution afforded dark brown crystals of **7**$[NiCl_4]\cdot CH_2Cl_2$ (41 mg, 0.023 mmol, 33% yield). In this case, concomitant formation of HCl was confirmed by trapping it as $HNEt_3Cl$ (54% yield based on **1**).

Synthesis of [(Cp*Ir)$_2$(μ_3-S)$_2$Ni(μ_3-S)$_2$(IrCp*)$_2$][BPh$_4$]$_2\cdot$0.5CH$_2$Cl$_2$ (7[BPh$_4$]$_2\cdot$0.5CH$_2$Cl$_2$). To a suspension of **7**$[NiCl_4]\cdot 0.5CH_2Cl_2$ (75 mg, 0.042 mmol) in THF (8 mL) was added $NaBPh_4$ (84 mg, 0.25 mmol), and the mixture was stirred at room temperature for 15 h. The solvent was removed in vacuo, and the residual solid was extracted with CH_2-Cl_2. Addition of hexane to the concentrated CH_2Cl_2 solution afforded **7**$[BPh_4]_2\cdot 0.5CH_2Cl_2$ (79 mg, 0.036 mmol, 86% yield) as brown crystals. Anal. Calcd for $C_{88.5}H_{101}B_2ClIr_4NiS_4$: C, 48.81; H, 4.67. Found: C, 48.89; H, 4.60. $\mu_{eff} = 3.01\ \mu_B$.

Reduction of 5[BPh$_4$]$_2$ to [(Cp*Ir)$_2$(μ_3-S)$_2$Fe(μ_3-S)$_2$(IrCp*)$_2$][BPh$_4$] (8[BPh$_4$]). To a suspension of **5**$[BPh_4]_2\cdot CH_2Cl_2$ (37 mg, 0.017 mmol) in THF (5 mL) was added Cp_2Co (6.6 mg, 0.035 mmol), and the mixture was stirred at room temperature for 15 h. The resulting dark brown solution was evaporated to dryness, and the residual solid was extracted with acetone. Addition of hexane to the acetone solution afforded **8**$[BPh_4]$ (14 mg, 0.077 mmol, 46% yield) as brown crystals. Anal. Calcd for $C_{64}H_{80}BFeIr_4S_4$: C, 42.40; H, 4.45. Found: C, 42.52; H, 4.51. $\mu_{eff} = 1.47\ \mu_B$.

Reduction of 6[BPh$_4$]$_2$ to [(Cp*Ir)$_2$(μ_3-S)$_2$Co(μ_3-S)$_2$(IrCp*)$_2$]-[BPh$_4$] (9[BPh$_4$]). To a suspension of **6**$[BPh_4]\cdot CH_2Cl_2$ (43 mg, 0.020 mmol) in THF (8 mL) was added Cp_2Co (3.8 mg, 0.019 mmol), and the mixture was stirred at room temperature for 15 h. The resulting solution was filtered, and addition of hexane to the filtrate gave **9**$[BPh_4]$ (15 mg, 0.0083 mmol, 44% yield) as dark brownish green crystals. ^{1}H NMR (δ, CD_2Cl_2, 20 °C): −12.67 (br, 60 H, Cp*), 6.87 (t, $J = 7.1$ Hz, 4 H, *p*-H of BPh_4), 7.02 (t, $J = 7.1$ Hz, 8 H, *m*-H of BPh_4), 7.30 (br, 8 H, *o*-H of BPh_4). At −60 °C, the Cp* signal shifts to δ −19.43. Anal. Calcd for $C_{64}H_{80}BCoIr_4S_4$: C, 42.32; H, 4.44. Found: C, 42.47; H, 4.48. $\mu_{eff} = 2.66\ \mu_B$.

Reduction of 7[BPh$_4$]$_2$ to [(Cp*Ir)$_2$(μ_3-S)$_2$Ni(μ_3-S)$_2$(IrCp*)$_2$][BPh$_4$] (10[BPh$_4$]). To a suspension of **7**$[BPh_4]_2\cdot 0.5CH_2Cl_2$ (46 mg, 0.021 mmol) in THF (5 mL) was added Cp_2Co (4.o mg, 0.021 mmol), and the mixture was stirred at room temperature for 15 h. The resulting dark brown solution was filtered, and addition of hexane to the filtrate gave **10**$[BPh_4]$ (28 mg, 0.015 mmol, 71% yield) as dark brown crystals. Anal. Calcd for $C_{64}H_{80}BIr_4NiS_4$: C, 42.33; H, 4.44. Found: C, 42.57; H, 4.46. $\mu_{eff} = 1.43\ \mu_B$.

X-ray Diffraction Studies. Single crystals of **3**, **4**, **5**$[BPh_4]_2\cdot CH_2$-Cl_2, **6**$[CoCl_3(NCMe)]_2$, **7**$[NiCl_4]\cdot CH_2Cl_2$, **8**$[BPh_4]$, **9**$[BPh_4]$, and **10**$[BPh_4]$ were sealed in glass capillaries under an argon atmosphere and used for data collection. Diffraction data were collected on a Rigaku AFC7R four-circle automated diffractometer with graphite-monochromatized Mo Kα radiation ($\lambda = 0.710\ 69$ Å) at 20 °C using the ω scan technique for **6**$[CoCl_3(NCMe)]_2$ and **7**$[NiCl_4]\cdot CH_2Cl_2$ and the $\omega-2\theta$ scan technique for **3**, **4**, **5**$[BPh_4]_2\cdot CH_2Cl_2$, **8**$[BPh_4]$, **9**$[BPh_4]$, and **10**$[BPh_4]$. The orientation matrixes and unit cell parameters were determined by least-squares refinement of 23 (for **4** and **5**$[BPh_4]_2\cdot CH_2Cl_2$) or 25 (for **3**, **6**$[CoCl_3(NCMe)]_2$, **7**$[NiCl_4]\cdot CH_2Cl_2$, **8**$[BPh_4]$, **9**$[BPh_4]$, and **10**$[BPh_4]$) machine-centered reflections with $32.3 < 2\theta < 37.8°$ for **3**, $37.7 < 2\theta < 39.5°$ for **4**, $33.0 < 2\theta < 36.2°$ for **5**$[BPh_4]_2\cdot CH_2Cl_2$, $33.7 < 2\theta < 39.8°$ for **6**$[CoCl_3(NCMe)]_2$, $22.5 < 2\theta < 36.8°$ for **7**$[NiCl_4]\cdot CH_2Cl_2$, $28.5 < 2\theta < 33.4°$ for **8**$[BPh_4]$, $33.9 < 2\theta < 39.4°$ for **9**$[BPh_4]$, and $36.8 < 2\theta < 39.9°$ for **10**$[BPh_4]$. Intensity data were corrected for Lorentz and polarization effects and for absorption (empirical, ψ scans).

Table 10. X-ray Crystallographic Data for **7**[$NiCl_4$]·CH_2Cl_2, **8**[BPh_4], **9**[BPh_4], and **10**[BPh_4]

	7[$NiCl_4$]·CH_2Cl_2	**8**[BPh_4]	**9**[BPh_4]	**10**[BPh_4]
empirical formula	$C_{41}H_{62}Cl_6Ir_4Ni_2S_4$	$C_{64}H_{80}BFeIr_4S_4$	$C_{64}H_{80}BCoIr_4S_4$	$C_{64}H_{80}BIr_4NiS_4$
fw	1782.18	1813.11	1816.20	1815.97
cryst syst	monoclinic	monoclinic	monoclinic	triclinic
space group	$P2_1/c$	$P2_1/c$	$P2_1/c$	$P\bar{1}$
cryst size, mm	0.60 × 0.40 × 0.40	0.25 × 0.40 × 0.40	0.20 × 0.50 × 0.60	0.25 × 0.30 × 0.50
a, Å	13.205(6)	19.649(4)	19.792(5)	15.445(6)
b, Å	17.303(8)	17.601(3)	17.522(5)	18.786(5)
c, Å	22.877(6)	20.321(3)	20.473(7)	11.891(2)
α, deg				99.93(2)
β, deg	92.95(3)	116.84(1)	117.17(2)	110.58(2)
γ, deg				76.35(3)
V, Å^3	5220(3)	6271(1)	6316(3)	3123(1)
Z	4	4	4	2
D_{calc}, g cm^{-3}	2.267	1.920	1.910	1.931
μ(Mo Kα), cm^{-1}	113.88	88.78	88.47	89.81
no. of unique rflns	9529	11428	11515	14367
no. of rflns used [$I > 3\sigma(I)$]	5564	7362	7157	8662
R^a	0.051	0.044	0.036	0.047
$R_w{}^b$	0.041	0.035	0.026	0.030
GOF^c	1.56	1.61	1.32	1.92

^{a} $R = \sum||F_o| - |F_c||/\sum|F_o|$. ^{b} $R_w = [\sum w(|F_o| - |F_c|)^2/\sum wF_o^2]^{1/2}$, $w = 1/\sigma^2(F_o)$. ^{c} GOF $= [\sum w(|F_o| - |F_c|)^2/(N_{obs} - N_{params})]^{1/2}$.

For crystals of **3**, **4**, **5**[BPh_4]$_2$·CH_2Cl_2, **6**[$CoCl_3$(NCMe)]$_2$, **7**[$NiCl_4$]·CH_2Cl_2, **8**[BPh_4], and **10**[BPh_4], no significant decay was observed for respective three standard reflections monitored every 150 reflections during the data collection. For compound **9**[BPh_4], slight decay (4.83%) was observed during the data collection, and a correction for decay was applied. Details of the X-ray diffraction study are summarized in Tables 9 and 10.

The structure solution and refinements were carried out by using the teXsan program package.[33] The positions of the non-hydrogen atoms were determined by Patterson methods (DIRDIF PATTY[34]) and subsequent Fourier syntheses. All non-hydrogen atoms were refined by full-matrix least-squares techniques with anisotropic thermal parameters except for the carbon and boron atoms of **5**[BPh_4]$_2$·CH_2Cl_2. The Cp* groups in **5**[BPh_4]$_2$·CH_2Cl_2 were found to be disordered to a minor extent, and the carbon and boron atoms of this compound were refined isotropically. Hydrogen atoms were placed at the calculated positions and were included in the final stage of refinements with fixed isotropic parameters.

Molecular Orbital Calculations. All molecular orbital calculations were performed on CAChe system by employing the extended Hückel method with the parameters taken from the literature,[35] where 3d orbitals of the sulfur atoms were not included in the calculations. The non-hydrogen atoms in the Cp analogues of **5**−**7**, [$(CpIr)_2(\mu_3\text{-}S)_2M(\mu_3\text{-}S)_2(IrCp)_2]^{2+}$ (M = Fe, Co, Ni), and the Cp analogue of **8**, [$(CpIr)_2(\mu_3\text{-}S)_2Fe(\mu_3\text{-}S)_2(IrCp)_2]^{+}$, were placed according to C_2-idealized structures with the dihedral angles between the two Ir_2M planes ranging from 0 to 180°; they are based on the observed structures of **5**[BPh_4]·CH_2Cl_2, **6**[$CoCl_3$(NCMe)]$_2$, **7**[$NiCl_4$]·CH_2Cl_2, and **8**[BPh_4], respectively.

Acknowledgment. This work was supported by a Grant-in-Aid for Specially Promoted Research (09102004) from the Ministry of Education, Science, Sports, and Culture, Japan. We also thank Professor Kazuyuki Tatsumi of Nagoya University for his helpful suggestions about the molecular orbital calculations.

Supporting Information Available: X-ray crystallographic files, in CIF format, for the structure determinations of **3**, **4**, **5**[BPh_4]$_2$·CH_2Cl_2, **6**[$CoCl_3$(NCMe)]$_2$, **7**[$NiCl_4$]·CH_2Cl_2, **8**[BPh_4], **9**[BPh_4], and **10**[BPh_4] are available on the Internet only. Access information is given on any current masthead page.

IC9806885

(33) *teXsan: Crystal Structure Analysis Package*; Molecular Structure Corp.: The Woodlands, TX, 1985 and 1992.

(34) PATTY: Beurskens, P. T.; Admiraal, G.; Beurskens, G.; Bosman, W. P.; Garcia-Granda, S.; Gould, R. O.; Smits J. M. M.; Smykalla, C. *The DIRDIF program system*; Technical Report of the Crystallography Laboratory, University of Nijmegen: Nijmegen, The Netherlands, 1992.

(35) (a) Hoffmann, R.; Chen, M. M. L.; Elian, M.; Rossi, A. R.; Mingos, D. M. P. *Inorg. Chem.* **1974**, *13*, 2666. (b) Schilling, B. E. R.; Hoffmann, R. *J. Am. Chem. Soc.* **1979**, *101*, 3456. (c) Alemany, P.; Hoffmann, R. *J. Am. Chem. Soc.* **1993**, *115*, 8290.